Iron Loss Modelling and Material Property Degradation

Effects of Cutting Techniques, Material Variations, and Sinusoidal vs. Non-Sinusoidal Flux Distribution

ULRIKA EINARSSON

EMELIE NYGREN

DEPARTMENT OF ELECTRICAL ENGINEERING

CHALMERS UNIVERSITY OF TECHNOLOGY

Gothenburg, Sweden 2024

www.chalmers.se

Master's thesis 2024

Iron Loss Modelling and Material Property Degradation

Effects of Cutting Techniques, Material Variations, and Sinusoidal vs. Non-Sinusoidal Flux Distribution

ULRIKA EINARSSON
EMELIE NYGREN

CHALMERS
UNIVERSITY OF TECHNOLOGY

Department of Electrical Engineering
Division of Electric Power Engineering
Chalmers University of Technology
Gothenburg, Sweden 2024

Iron Loss Modelling and Material Property Degradation
Effects of Cutting Techniques, Material Variations, and Sinusoidal vs. Non-Sinusoidal Flux Distribution
ULRIKA EINARSSON
EMELIE NYGREN

Supervisor: Sima Soltanipour, Volvo Cars Corporation
Examiner: Torbjörn Thiringer, Electric Power Engineering

Master's Thesis 2024
Department of Electrical Engineering
Division of Electric Power Engineering
Chalmers University of Technology
SE-412 96 Gothenburg
Telephone +46 31 772 1000

Typeset in LaTeX
Gothenburg, Sweden 2024

Iron Loss Modelling and Material Property Degradation
Effects of Cutting Techniques, Material Variations, and Sinusoidal vs. Non-Sinusoidal Flux Distribution
ULRIKA EINARSSON
EMELIE NYGREN
Department of Electrical Engineering
Chalmers University of Technology

Abstract

With the electric vehicle industry expanding rapidly, there is an increasing demand for high efficiency in electric machines (EM). In order to achieve that, there is a need to have precise modeling of the EM and its losses. In this thesis, the iron loss degradation in EMs due to cutting during the manufacturing process is studied. Measurements were conducted on laminates of electrical steel with sinusoidal and Pulse Width Modulated (PWM) flux density and the results were analysed and compared. Further, measurements on materials cut with punching and laser cutting were compared as well as materials cut in the transversal and length directions. The results from the measurements were used to model the degradation and iron losses and to perform a Finite Element Method (FEM) simulation of a Permanent Magnet Synchronous Machine (PMSM) with sinusoidal current excitation in Ansys Maxwell.

From the measurements, it was concluded that all investigated materials were degraded due to cutting during the manufacturing process. The materials that had been cut using punching had better magnetic properties and lower losses than the ones that had been laser cut. The samples cut in the length direction showed significantly higher permeability than the ones cut in the cross direction but had higher degradation effects when compared to the uncut material. The effect of thickness on the sheet were compared for one punched material, the result is that thinner materials had better magnetic properties than thicker ones. However, the thicker materials were less affected by degradation when compared to the uncut material of the same thickness. The measurements with PWM had substantially higher losses than the sinusoidal measurements but the degradation effects were similar for both types of feeding. PWM feeding with higher frequency modulation ratio and higher modulation index both yield lower losses. From the FEM simulations, it was seen that the degraded machine models showed an increase in iron losses of up to 24 % which resulted in a decrease in efficiency of up to 0.12 percentage points.

Keywords: iron losses, electric machine, punching, laser cutting, PWM, SST, Epstein frame, FEM, degradation, manufacturing effects

Acknowledgements

First and foremost we would like to thank our supervisor, PhD student Sima Soltanipour for her help, support and advice throughout the thesis. She always brought a positive attitude and we wish her all the best in her future PhD studies. Then we would like to give our thanks to our examiner, professor Torbjörn Thiringer for his guidance, advice and always finding the time in your busy schedule. We would also like to show our gratitude to Anders Thulin and Volvo Cars Corporation for the opportunity to get to know the company and get an insight in the industry.

Finally a big thank you to all of the friends that we have made here at Chalmers throughout our five years. It really would not have been as memorable or such a great experience without you all. We have been through ups and downs together, and now we wish you a big good luck in the future as engineers.

Ulrika Einarsson & Emelie Nygren, Gothenburg, June 2024

List of Acronyms

EM	Electric Machine
FEM	Finite Element Method
FFT	Fast Fourier Transform
IEC	International Electrotechnical Commission
PMSM	Permanent Magnet Synchronous Machine
PWM	Pulse Width Modulation
SST	Single Strip Tester
WLTC	Worldwide Harmonised Light Vehicle Test Cycle

Nomenclature

A	Cross-sectional area
B	Magnetic flux density
C_d	Aerodynamic drag coefficient
C_m	Fitting coefficient Steinmetz equation
C_r	Rolling resistance coefficient
d	Thickness of electrical steel
f	Fundamental frequency
f_r	Frequency modulation ratio
H	Magnetic field strength
H_{deg}	Magentic field strength degradation
$i(t)$	Current over time
k_{ec}	Eddy current loss coefficient
k_{ex}	Excess loss coefficient
k_h	Hysteresis loss coefficient
l_m	Length of the magnetic path
m	Mass
m_a	Modulation index
N	Number of turns
P_s	Specific power loss
$P_{s,deg}$	Specific power loss degradation
r	Radius
T	Time period
T_e	Torque
$u(t)$	Voltage over time
U	Voltage
v	Top speed

α	Fitting coefficient Steinmetz equation
β	Fitting coefficient Steinmetz equation
σ	Conductivity
ρ	Density
μ_r	Relative permeability
ω	Angular frequency

Contents

1
Introduction

The climate crisis has become a widely discussed topic and the transport sector accounted for 25 % of the total emissions in Europe year 2023 [1]. As an attempt to reduce the emissions, the electric vehicle industry has developed and expanded. The interest for electric cars has increased significantly and as a result, this industry has become extensively more competitive and the demand for high efficiency is important. To be able to obtain that efficiency, there is a need of precise modeling of the losses in the electric machine (EM) used for the electric vehicle.

1.1 Background

One part of the loss model for the EM that could improve in accuracy is the loss that appears due to the electromagnetic properties in the iron core, also called the iron losses. When modelling iron losses, the general method is to use parameters from a data sheet for the specific steel used in the iron core. These data sheets are not including the manufacturing effects that appear in the steel when manufacturing the core of the stator and rotor. The material will be degraded during the manufacturing and the losses will increase compared to using the data sheet values [2].

Another important point is that data sheet parameters are derived from a sinusoidal flux density [3]. In electric vehicles, Pulse Width Modulation (PWM) is one of the most common types of feeding for the EM [4]. If the loss model is based on parameters from a data sheet, the effects on the degradation as well as magnetic properties of the material when using non-sinusoidal feeding will not be considered. Thus, a more accurate loss model can be attained by studying these effects.

1.2 Previous work

There have been several studies regarding how much the manufacturing process affects the material properties and iron losses in EM. In [2], it is concluded that losses can increase by 6 % for low degradation and 22 % for high degradation. However, according to [5], they can increase by 30-40 %. Most studies conclude that the manufacturing does have an impact on materials and losses but the extent of the effects varies between them. These differences are due to the use of different materials and methods.

Although there are some differences in how the previous studies have been carried out, most of them are similar in that they have been done using sinusoidal feeding of flux density. Looking at how PWM feeding affects the iron losses due to degradation from the manufacturing is something that has not been studied a lot. There are, however, some studies which have considered PWM feeding. In [6] and [7], it is concluded that using PWM feeding increases the iron losses in EMs, and according to [6], that increase can be up to 30 %.

A previous master's thesis investigated the effects of manufacturing on the iron losses of a Permanent Magnet Synchronous Machine (PMSM) fed with sinusoidal and PWM signals [8]. That thesis only investigated one cutting method on one material. This report will include comparisons of several materials, three cutting methods and non-sinusoidal feeding. It will also look at how the direction of the cut affects the material. Lastly it will further develop the loss model for a Finite Element Method (FEM) implementation.

1.3 Purpose

The purpose of this thesis is to study the degradation effect on electrical steel due to manufacturing. The following objectives will be evaluated:

- Comparing the cutting techniques: punching, industrial laser cutting and state of the art laser cutting.
- Comparing the impact of cutting in the transversal and length direction.
- Comparing the magnetic properties and degradation between thinner and thicker steel sheets.
- Evaluating the differences of sinusoidal and non-sinusoidal flux distribution.
- Modelling the degradation effect for FEM implementation.
- Implementation and simulation in FEM software.

This is done by carrying out measurements and analysing the results. Furthermore, the measurement results with sinusoidal feeding are to be used to model the degradation and losses and will then be implemented in a FEM simulation of an EM in Ansys Maxwell.

2
Theory

In this chapter, the theory that serves as the basis of this thesis is presented. It includes the origins, measurement methods and modelling of iron losses as well as manufacturing methods of stator and rotor cores and at last the working principle of PWM.

2.1 Iron losses

The losses in an EM consists of three types of losses: mechanical losses, copper losses and iron losses. The mechanical losses originate from friction losses in the bearings and the windage losses in the moving machine parts. The mechanical losses have a strong dependency on speed and increase with speed. The copper losses are the losses that occur due to the current in the windings of the machine. The copper losses depend primarily on the magnitude of the current and the resistance in the windings. The iron losses are the losses that occur in the stator and rotor core due to the changing magnetic field [6].

The iron losses can be divided into three parts: hysteresis losses, eddy currents losses and excess losses. The iron losses are especially difficult to model since they can not be directly measured. The break down of the iron losses do not represent the physical phenomena but is more of an engineering method to fit the modelling of the losses.

2.1.1 Hysteresis losses

The material of the stator and rotor core has a non linear relation between the magnetic field strength H and the magnetic flux density B. The relation forms a hysteresis loop. The physical background is not fully understood, however, an explanation model is as following: ferromagnetic materials consists of domains, of small regions, and if there is no external excitation applied on the material, these regions are randomly arranged resulting in a net magnetic field of zero. Then when a magnetic field is applied, the domains of the material will align with the magnetic field and the material will be magnetized. With increasing H the magnetic flux density will increase until it reaches saturation, which is represented by point I in Figure 2.1. When removing the magnetic field, the domains will not revert to the initially random state and B will not reach zero, the material will continue to remain slightly magnetized, point II. The remaining flux density is called remanence and an

opposite magnetic field is needed to remove it. The total magnetic field needed to remove all of the remanence is called the coercivity. If the magnetic field is increased further in the negative direction the magnetic flux will once again reach saturation at point III [9][10].

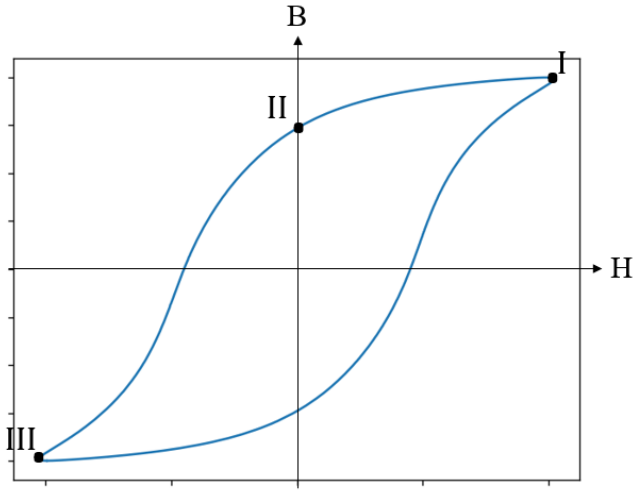

Figure 2.1: Hysteresis loop of ferromagnetic material.

The hysteresis losses are proportional to the enclosed area of the loop which represents the specific energy for each cycle. A larger area yields a greater hysteresis loss. The loop represents the relation between H and B that is specific for a certain material and it will change according to the materials permeability and reluctance [6].

2.1.2 Eddy currents losses

Eddy current losses come from the induced electric currents within the material that originates from the time varying magnetic field. These induced currents will circulate at the surface of the material causing energy to be dissipated as heat depending on the material resistivity. The eddy currents losses are proportional to the square of the excitation frequency as well as the square of the flux density [9].

The eddy current losses can be decreased by dividing the core into thin layers along the axial length. This will create smaller areas and higher resistance which yields lower eddy currents for the same induced voltage. In addition, the eddy currents could be decreased by including a material, typically silicon, to the core material and in that way increase the resistivity and reduce the eddy current [10].

2.1.3 Excess losses

The excess loss is often considered when modelling the iron losses and is commonly referred to the difference between the total magnetic loss and the hysteresis and eddy currents losses. They can also be referred to as the anomalous losses. The

excess loss is the least significant among the iron losses and is mainly originating from movements in the domain wall when magnetizing the material. It gives rise to local flux changes which induce small eddy currents [11].

2.2 Iron loss modelling

There are numerous iron loss models used, some rather simple and other more complex modelling methods. This section gives the background to the model utilized in this thesis as well as the FEM program Ansys Maxwell.

Firstly there is a group of models based on the Steinmetz Equation

$$P_s = C_m f^{\alpha} \hat{B}^{\beta} \tag{2.1}$$

where P_s is the specific power loss in W/kg, f is the fundamental frequency, $\hat{B}$ is the peak flux density of the material, and C_m, α and β are fitting coefficients for the model and are determined from measurement data. There are modifications of the Steinmetz equation yielding new models such as Generalized Steinmetz Equation and improved General Steinmetz equation. However, all of the modifications of the Steinmetz equation have a problem in common and it is that the coefficients vary with frequency. It can therefore be hard to find applicable coefficients for the full frequency range, especially for waveforms with high harmonic content.

Ansys Maxwell uses the Bertotti model which uses the approach to separate the iron losses based on the Steinmetz equation into three parts: hysteresis loss, eddy currents loss and excess loss. The total loss becomes

$$P_s = P_h + P_{ec} + P_{ex} = k_h f B_m^2 + k_{ec} f^2 B_m^2 + k_{ex} f^{1.5} B_m^{1.5} \tag{2.2}$$

where k_h, k_{ec} and k_{ex} are the fitting coefficients for the hysteresis loss, eddy currents loss and excess loss respectively. All parts of the losses have a dependency on the frequency, hysteresis losses are directly proportional while the eddy current losses are proportional to the frequency squared and the excess losses are proportional to the frequency to the power of 1.5. It can be assumed that at low frequencies, f $\rightarrow$ 0 Hz, only hysteresis losses are present and that the hysteresis losses are proportional to the area of the hysteresis loop of the material at low frequencies.

The eddy current coefficient of the losses can be physically derived using Maxwell's equation as

$$k_{ec} = \frac{\sigma \pi^2 d^2}{6\rho} \tag{2.3}$$

where σ is the conductivity, d is the thickness of the electrical steel and ρ is the density of the material.

2.3 Measurement methods

In order to measure magnetic properties in electric steel sheets, there are several different techniques that can be used. The Epstein frame is the most commonly used one but the Single Sheet Tester and the ring core set-up are common as well. Magnetic properties of a material include the magnetic field strength, H, the magnetic flux density, B and the specific power loss, P_s. The magnetic field strength can be found using Ampere's law as

$$H(t) = \frac{N_1 i(t)}{l_m} \tag{2.4}$$

where N_1 is the number of turns in the primary windings, $i(t)$ is the current over time and l_m is the length of the magnetic path. The induced voltage in the secondary winding can then be used to calculate the flux density using Faraday's law as

$$\frac{dB}{dt} = -\frac{u_2(t)}{N_2 A_m} \implies B(t) = -\frac{1}{N_2 A_m}\int_0^t u_2(t)dt \tag{2.5}$$

where $u_2(t)$ is the voltage of the secondary winding, N_2 is the number of turns in the secondary winding and A_m is the cross-sectional area of the steel strip. Furthermore, the material's specific power loss can be calculated as

$$P_s[\mathrm{W/kg}] = \frac{f}{\rho}\int_0^T H dB \tag{2.6}$$

where f is the frequency, ρ is the density, T is the time period, H is the magnetic field strength and B is the magnetic flux density. In order to have a sinusoidal voltage at the secondary winding, the form factor should be equal to 1.11. The form factor can be described as

$$FormFactor = \frac{V_{RMS}}{V_{average}} = \frac{\sqrt{\frac{1}{T}\int_0^T \hat{V}^2 \sin(\omega t)^2 dt}}{\frac{1}{T}\int_0^2 \hat{V}\sin(\omega t)dt} \tag{2.7}$$

where V_{RMS} is the RMS voltage, $V_{average}$ is the average voltage, T is the time period, $\hat{V}$ is the peak voltage and ω is the angular frequency.

2.3.1 Epstein Frame

The Epstein frame is shaped as a square with four coils, one along each side of the square, consisting of primary and secondary windings connected in series [12]. Steel strips to be tested are then placed inside this square with overlapping ends and thus the number of test strips should always be a multiple of four. This setup can be seen in Figure 2.2. Due to the overlapping corners, there will be some leakage flux which is a disadvantage with the Epstein frame. To reduce the leakage flux, weights are usually placed on top of these corners.

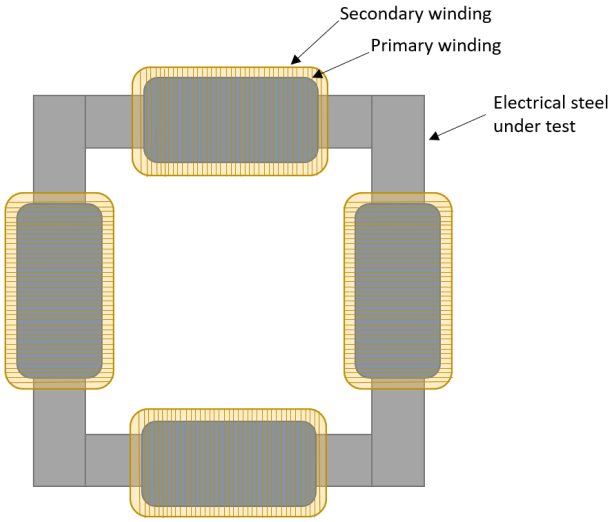

Figure 2.2: The Epstein frame from a top view.

Measuring with the Epstein frame follows the International Electrotechnical Commission's (IEC) standard IEC60404-2 and according to that, the width of the steel sheet to be tested should be 30 mm and its length should be between 280 mm and 320 mm [4]. Further, an inductor can be used to compensate for the air flux.

2.3.2 Single Strip Tester

As mentioned previously, another measurement method standardised by the IEC is the Single Sheet Tester. With this method, a large steel sheet is placed between two yokes and measured according to the standard [13]. The Single Strip Tester (SST) follows the same standard but measures on smaller steel strips instead of larger sheets and is the method that is used in this thesis. The strips should be 30 mm wide and at least 280 mm long. The windings for an SST can either be wound on the two yokes or on a bobbin along the sheet to be tested. Both of these set-ups can be seen in Figure 2.3.

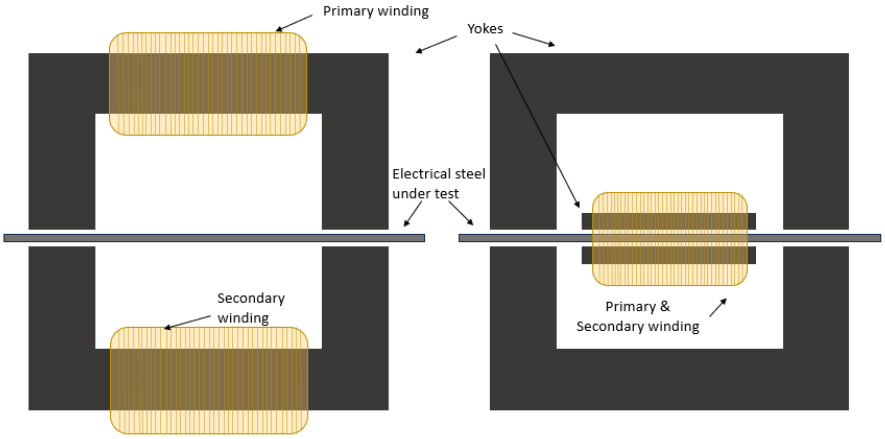

Figure 2.3: The SST from a side view with the windings on the yokes (left) and on a bobbin along the test strip (right).

The equipment used in this thesis uses the second option, which is to the right in the figure. A difference between the Epstein frame and the SST is that the SST only needs one steel strip, while the Epstein frame needs at least four.

2.4 Manufacturing

During the manufacturing process of the stator and rotor in EMs, laminated electrical steel sheets are first cut into a desired shape and then joined together. The purpose of using these thin laminations is to minimize eddy current losses [14]. The cutting process is usually the part of the manufacturing that has the largest effect on degradation [15]. Two of the most common cutting techniques are punching and laser cutting which will be described below. Other methods for the cutting process are water jet cutting where highly pressurized water is directed through a thin nozzle [16] and electric discharge machining where electric sparks are created and used to remove material [17].

2.4.1 Punching

When it comes to mass-production of EMs, punching is the most common method of cutting [18]. With this technique, a cutting tool with a geometry specific to the design is used to punch out the desired shape in the material. Therefore, the initial cost is high but for large-scale production, the total cost is low compared to other methods. An advantage with punching is that there is no thermal stress applied to the material. There is however, mechanical stress. Punching causes plastic deformation around the cut edge which affects the material's magnetic properties and causes an increase in iron losses [19]. Different factors including the geometry of the cut, sharpness of the tool and properties of the material decide how large the deteriorating effects will be.

2.4.2 Laser cutting

Laser cutting is, contrary to punching, not often used in mass-production. Instead, it is most commonly used for prototyping as well as smaller batches of EMs. This is both due to that it is a time consuming process and also since it is easy to quickly, and at a low cost, modify the geometry of the cut [20]. With this technique, a laser is used to cut the material into the desired shape. Heat is applied to the specific area to be removed, causing it to turn into a gas or liquid. This means that there is some thermal stress added to the material which affects its properties and increases iron losses [21]. Factors that affect to what extent laser cutting will contribute to the deterioration of the material include the geometry of the cut, the material and the type of laser used.

2.5 Pulse Width Modulation

A switching method that is common to use with EMs is PWM. Using this method, a desired reference wave is compared to a triangular wave with a higher frequency, called the carrier wave. When the reference signal is above the carrier wave, the PWM signal is equal to half of the DC voltage and the upper part of the inverter circuit is switched on. When the carrier wave is above the reference wave, the PWM signal becomes the same value but negative and the lower part of the inverter circuit is switched on while the upper part is switched off [22]. The reference and carrier waves as well as the resulting PWM signal can be seen in Figure 2.4.

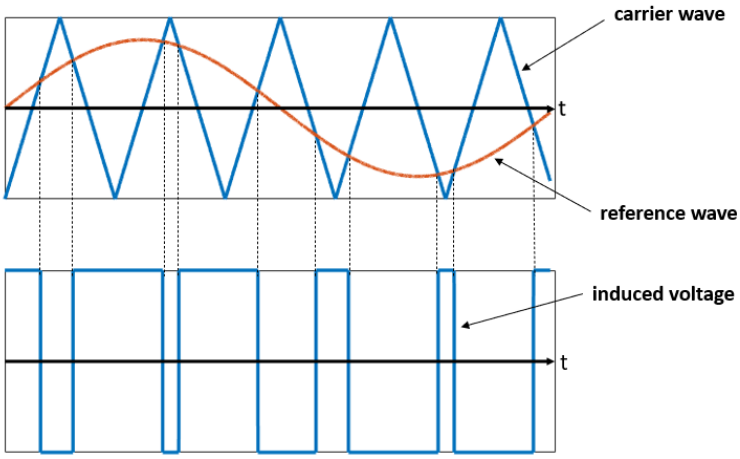

Figure 2.4: The reference and carrier wave in PWM control and the resulting PWM signal.

The triangular carrier wave is determined by the modulation index m_a and the frequency modulation ratio f_r. The modulation index is the ratio between the amplitudes of the reference and carrier waves and is defined as

$$m_a = \frac{\hat{V}_{reference}}{\hat{V}_{carrier}} \tag{2.8}$$

where $\hat{V}_{reference}$ is the amplitude of the reference signal and $\hat{V}_{carrier}$ is the amplitude of the carrier wave. Usually the modulation index is less than or equal to one, meaning that the modulation is linear. However, if it is greater than one, i.e. if the amplitude of the reference is greater than the amplitude of the carrier wave, it is overmodulated. This means that there is no longer linearity in the modulation and the output and reference voltages are not linearly proportional. Overmodulation also leads to unwanted harmonics in the resulting PWM signal [22]. Furthermore, the frequency modulation index should be an odd number and a multiple of three. The frequency modulation ratio is the ratio between the frequency of the carrier wave, or the switching frequency, and the frequency of the reference wave is described as

$$f_r = \frac{f_{carrier}}{f_{reference}} \tag{2.9}$$

where $f_{carrier}$ is the switching frequency and $f_{reference}$ is the frequency of the reference signal.

3

Case set-up

This project was executed in two parts, measurements and simulations, where the results from the measurements were implemented in the simulations.

The machine modeled in the simulations is suitable for a mid-sized electric car. Therefore a drive cycle assessment was done with a mid-size example car to obtain interesting and appropriate operating points. The result from the analysis can be seen in Figure 3.1. The parameters used for the drive cycle assessment are presented in Table 3.1 [23]. The drive cycle is WLTC which is the Worldwide Harmonised Light Vehicle Test Cycle.

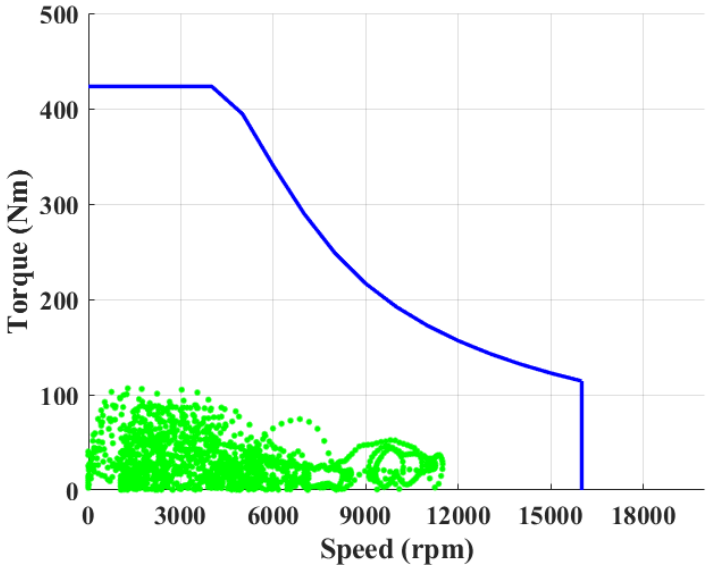

Figure 3.1: Representation of the WLTC drive cycle in the speed-torque map of the simulated EM and with a midsize car as reference. The green dots represents the points of the drive cycle.

Table 3.1: Parameters used for the drive cycle.

Parameter	Symbol	Unit	Value
Aerodynamic drag coefficient	C_d		0.32
Effective cross sectional area	A_f	$[m^2]$	2.61
Rolling resistance coefficient	C_r		0.009
Mass	m	[kg]	2100
Radius of wheel	r	[m]	0.3
Top speed	v	[km/h]	180
Gear ratio			9.9

The operating points were obtained from Figure 3.1 and are presented in Table 3.2. One of the points is chosen at low speed and torque and the other two points are at higher speed and torque levels.

Table 3.2: Operating points observed in the simulations.

Speed [rpm]	Torque [Nm]	Frequency [Hz]
3000	100	200
3000	250	200
9000	100	600

3.1 Measurement set-up

The measurements were done to investigate and compare the magnetic properties and specific power loss for different materials, manufacturing methods and different excitations. To be able to see the effect of degradation due to cutting during the manufacturing process, five samples with different amounts of cuts were measured. These samples were all of the size 30x300 mm except for the laser cut NO25 material which was 30x280 mm. Each sample type had different widths between each cut and their geometries can be seen in Figure 3.2. Sample A only has one cut on each side and will be used as a reference against the other samples.

The main material throughout this thesis is NO25 with the punched cutting technique and a thickness of 0.25 mm, this material will be used as the reference for a lot of comparisons. The rest of the materials that will be included in the material comparison are presented in Table 3.3. The evaluation will include a comparison of punching and laser cutting, the thickness of the sample and if the sample is cut in the rolling direction when the steel sheet is manufactured i.e. the length direction, or in the transversal direction. Regarding the laser cutting, two different cutting methods will be evaluated: industrial laser and state of the art laser. The material cut with the industrial laser, which purpose is not to cut steel for EMs, is referred to as NO25_1 Laser. The material cut with a state of the art laser which is meant to cut steel for EMs is referred to as NO25_2 SOTA and is a different material than the other laser cut material. NO27 is a material that has a different composition of silicon in the material.

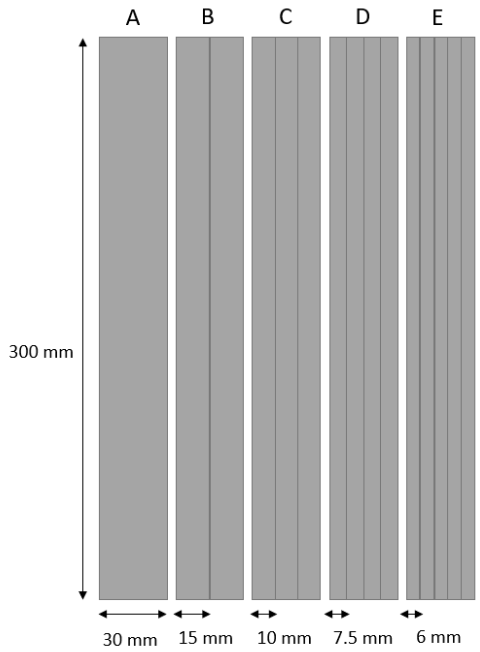

Figure 3.2: Samples used for measurements.

Table 3.3: Properties of the materials used for the material comparison

Material/Name	Thickness [mm]	Transversal/Length
NO25_1 Punched	0.25	Transversal
NO25_1 Laser	0.25	Transversal
NO25_2 SOTA	0.25	Transversal
NO35_1 Punched	0.35	Transversal & Length
NO27_3 Punched	0.27	Length

The measurement method has been varied between the samples and the materials. The Epstein frame is the preferable choice but it requires more samples to measure on than the SST which only requires one sample to do the measurement. The Epstein frame has been used in those cases where it has been possible and when there have not been enough samples, the measurements have been done with the SST instead. Table 3.4 presents the measurement method for each sample and material. For the measurements with Epstein frame, 12 samples were used.

Table 3.4: Measurement method used for each sample and material.

Material/Name	Epstein Frame	SST
NO25_1 Punched	sample A-D	sample E
NO25_1 Laser	sample A-E	
NO25_2 SOTA	sample A	sample B-E
NO35_1 Punched	sample A-C	sample D-E
NO27_3 Punched	sample A-D	sample E

The strips of electrical steel were measured using equipment from Brockhaus along with the MPG Expert software. The Epstein frame from Brockhaus has four different winding configurations. The configurations each have different limitations in frequency, flux density and field strength [24] and these can be found in Table 3.5.

Table 3.5: Epstein winding configurations.

Winding	Frequency	Flux Density	Field Strength
700	3-150 Hz	0.001-2 T	5-30 000 A/m
200	150-2 000 Hz	0.005-1.8 T	0-5 000 A/m
60	1-5 kHz	0.001-2 T	5-3 000 A/m
20	2.5-20 kHz	0.001-2 T	0-1 000 A/m

Once the samples have been placed in the Epstein frame or SST, MPG-Expert is used to do the desired measurements. In the software, a target value of polarisation as well as a desired signal shape is chosen and then it controls the output to fit those requirements. Then the frequency is chosen for the measurement and once the measurements are finished, the results from MPG-Expert are post-processed. In this thesis, the measurements have sequences of polarisation as the reference values that MPG-Expert controls the signal to. The measurement setup for sinusoidal feeding for NO25 punched can be seen in Table 3.6. More measurements were done on NO25 punched to get a overview of the behaviour, the rest of the materials have been measured at the two operating points, 200 Hz and 600 Hz.

Table 3.6: Measurement setup for sinusoidal feeding.

Frequency [Hz]	Winding	B_{start} [T]	B_{step} [T]	B_{stop} [T]
10	700	0.1	0.1	1.9
50	700	0.1	0.1	1.9
100	700	0.1	0.1	1.9
200	200	0.1	0.1	1.6
300	200	0.1	0.1	1.6
400	200	0.1	0.1	1.6
500	200	0.1	0.1	1.6
600	200	0.1	0.1	1.6
700	200	0.1	0.1	1.6
800	200	0.1	0.1	1.6
1 000	60	0.1	0.1	1.4
2 500	60	0.1	0.1	1.4
5 000	20	0.1	0.1	1.2
10 000	20	0.1	0.1	0.8
15 000	20	0.1	0.1	0.6
20 000	20	0.1	0.1	0.4

MPG-Expert can produce PWM feeding which has been used for the measurements for the non-sinusoidal comparison. When measuring with PWM feeding the modulation index m_a and frequency modulation ratio f_r are set for the measurement.

In MPG-Expert, they are decided by choosing the parameters V_r and F_{ha} which are defined as

$$V_r = \frac{1}{m_a} \tag{3.1}$$

$$F_{ha} = m_f \tag{3.2}$$

but m_a and f_r will be referred to instead in this thesis. Furthermore, a fundamental frequency of 50 Hz is chosen for the PWM feeding due to ripple in the measurement for higher frequencies. The measurements for PWM have been done with the Epstein frame with the 60 winding configuration for sample A-D and with the SST for sample E. The results will be compared to sinusoidal feeding at 50 Hz.

The modulation index for the EM varies with different loads. For the EM used in this project, the modulation index for each value of torque and speed can be seen in Figure 3.3. As the measurements are done at 50 Hz which corresponds to a speed of 750 rpm, the modulation index should be m_a=0.2. The measurement equipment was not able to measure for lower values than 0.3 and therefore m_a=0.3, 0.4 and 0.5 are investigated as well as f_r=9, 11, 15, 99 and 199.

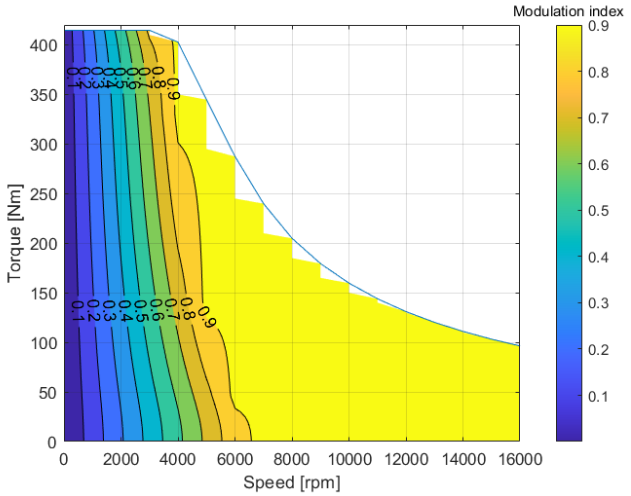

Figure 3.3: Modulation index for the EM.

MPG-Expert is used to carry out the measurements, a target value of polarisation is chosen and then the output is controlled to get the desired polarisation. Ripple in the polarisation will occur when having PWM feeding and when the peak of that ripple reaches the chosen polarisation, the software will consider it as reached. Therefore, the fundamental B-level will be lower than what is assigned in the measurement. Lower values of f_r have higher ripple and are therefore affected the most. To get the measurements to have the same fundamental B-level, different polarisations were assigned for the measurements. The measured polarisation for each f_r and the sinusoidal measurement used for comparison are presented in Table 3.7.

Table 3.7: Polarisation measured for PWM feeding.

f_r	B_{start}	B_{stop}
9	0.1	1.4
11	0.0935	1.309
15	0.0856	1.1984
99	0.0671	0.9394
199	0.0674	0.9436
sin	0.0642	0.8988

For comparison of the power losses between PWM feeding and sinusoidal feeding, the PWM loss was recreated using sinusoidal data for each harmonic of the PWM measurement. An FFT of the flux density shows the harmonic components of B at different frequencies. By obtaining the frequencies and B-values for the harmonics at a specific B-level, it should be possible to recreate the loss using the sinusoidal measurement with the same specifications and adding them together. Many of the B-values were so low that they could not be measured with the measurement equipment, in those cases the loss has been obtained by extrapolating the loss curves for that frequency. For low values of f_r the six first harmonic components have been included in the recreation, while at f_r=99 the three first components are included and at f_r=199 only the switching component was included. This is because the B-value got so low.

3.2 Simulation set-up

The EM model was simulated in the FEM-based simulation program Ansys Maxwell. It has been divided into two parts, a non-degraded model and one where the degradation from the measurements is implemented.

3.2.1 Machine model

The modeled EM was a Permanent Magnet Synchronous Machine (PMSM) with eight poles and a double layer of magnets. Since the EM consists of eight symmetric poles, it could be represented by one-eighth of the EM, to reduce computation time. Figure 3.4 shows the geometry of one of the poles.

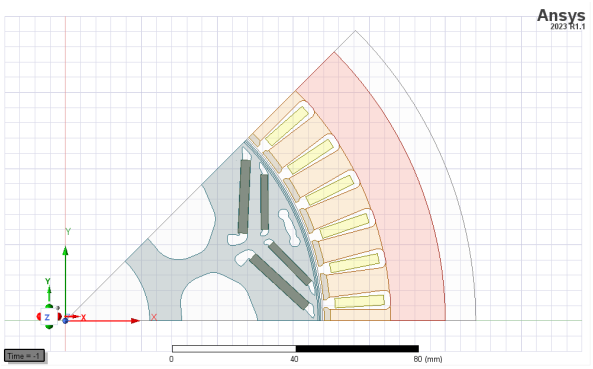

Figure 3.4: The EM model simulated in Ansys Maxwell.

The stator and windings were made using the built in RMxprt-tool from Ansys. The stator used the SlotCore and the windings used the LapCoil. The core was made using a circle and the magnets were made using a predefined IPMcore from RMxprt. The IPMcore was also used to make the cut-outs to fit the magnets into the rotor core. Futhermore, polylines were created to make the rest of the cut-outs for air which can be seen in Figure 3.4. The general parameters for the EM are presented in Table 3.8.

Table 3.8: General parameters for the geometry of the EM.

Parameter	Value	Unit
Rotor inner diameter	55.5	mm
Rotor outer diameter	168.2	mm
Stator inner diameter	170.4	mm
Stator outer diameter	250	mm
Number of slots	48	
Number of poles	8	

The EM was fed by a sinusoidal current excitation. The specifications concerning the EM and its performance are presented in Table 3.9.

Table 3.9: EM specifications

Parameter	Symbol	Value	Unit
Maximum Torque	$T_{e,max}$	420	Nm
Maximum Speed	ω_{max}	16000	rpm
Maximum RMS Current	I_{max}	650	A
Maximum voltage	U_{max}	370	V

3.2.1.1 Material

The EM consists of three different materials. The coils are made from copper, the magnets are made from neodymium bars as well as dysprosium and the stator and rotor cores are made from silicon steel. The specifications for the materials are presented in Table 3.10. The silicon steel for the stator and rotor cores have a nonlinear relation between the flux density and the magnetic field magnitude, this relation will be measured and then the measured values will be implemented in the EM. Four simulations with different silicon steel materials will be done, with non-degraded punched NO25, degraded punched NO25, non-degraded laser cut NO25 and degraded laser cut NO25. Since the measurements are averages across the samples, sample A, which is considered to be non-degraded, will not actually be completely non-degraded. Further, sample A for the punched and laser cut NO25 will not have the exact same values because of this and that is the reason two different non-degraded simulations will be done, one with the punched material and one with the laser cut material.

Table 3.10: Material for each part of the EM.

Part	Parameter	Symbol	value	Unit
Stator/	Stator/Rotor core material		NO25	
Rotor	Mass density	ρ_{fe}	7600	kg/m^3
Magnets	Magnet material		$N36Z\_20$	
	Relative permeability	μ_r	1.03	
	Bulk conductivity	σ	625000	S/m
	Magnetic field magnitude	H	-920000	A/m
Coil	Coil material		Copper	
	Relative permeability	μ_r	0.999991	
	Bulk conductivity	σ	58000000	S/m
	Mass density	ρ_{cu}	8933	kg/m^3

3.2.2 Degraded machine model

To simulate how the EM is affected by the degradation of the material, a degraded EM model was created. First, a mathematical model was developed and then that was implemented in Ansys Maxwell as in Figure 3.5. The modeled degraded material was put in the area from the cut edge to 1 mm from the cut edge in the stator and the measured non-degraded material was put in the rest of the core. The degradation in the rotor was not considered in this thesis due to that the losses in the rotor is significantly lower than in the stator. The EM model in Figure 3.5 was also used for the non-degraded simulations but with the non-degraded material everywhere in the stator. That is so that the mesh is the same for all simulations, since that could affect the results otherwise.

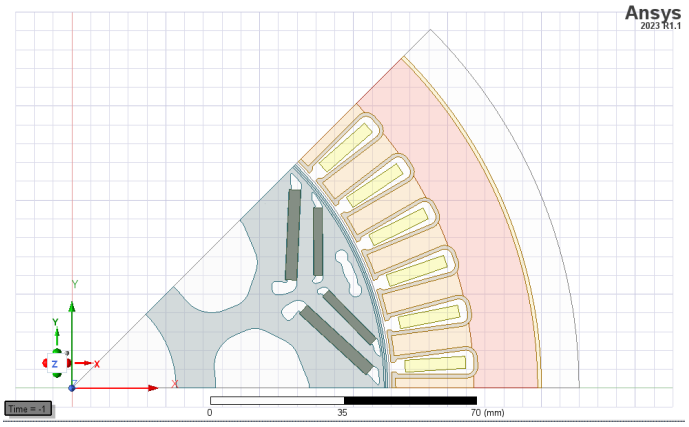

Figure 3.5: The degraded EM model in Ansys Maxwell.

In order to implement the degradation in Ansys, a mathematical model for the degradation up to 1 mm from the cut edge was developed. The measured values of the samples are averages for the specific width of the sample. To relate the width of each sample to a distance from cut edge, each sample width was divided by two so that the distance from cut edge is half of the sample width. The smallest width measured was 6 mm, which means that the distance from cut edge is 3 mm.

Therefore, there were no measurements at 1 mm from the cut edge so a model was needed to obtain that value. To do that, the magnetic field strength degradation and specific power loss degradation results were plotted against distance from the cut edge and curve-fitted for each B-value according to

$$H_{deg} = a_h \cdot e^{-b_h x} + c_h \tag{3.3}$$

$$P_{s,deg} = a_p \cdot e^{-b_p x} + c_p \tag{3.4}$$

where x is the distance from the cut edge and a, b and c are curve-fitting coefficients. The simulations were done with punched and laser cut NO25 and the same method was used for modelling both materials but the figures in this sections are based on the laser cut material. The resulting modeled H and P_s degradation versus distance to the cut edge at 200 Hz, $B = 1$ T and the measured degradation can be seen in Figure 3.6.

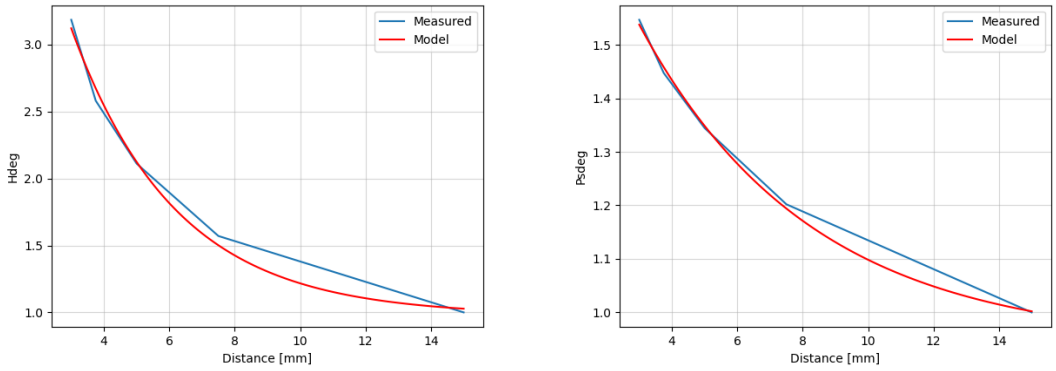

Figure 3.6: Modeled and measured H and P_s degradation vs distance to cut edge at 200 hz and $B = 1$ T with sinusoidal feeding for laser cut NO25.

The model was tested by applying it to the distances corresponding to samples B-E. The modeled and measured degradation for each B-value for sample E, which is the most degraded sample, at 200 Hz can be seen in Figure 3.7. The largest difference between the modeled and measured H degradation is 2.3 % and for the P_s degradation, the largest difference is 0.7 %. For the punched material, the largest difference between the modeled and measured curves for sample E is 2 % for the H degradation and 6 % for the P_s degradation.

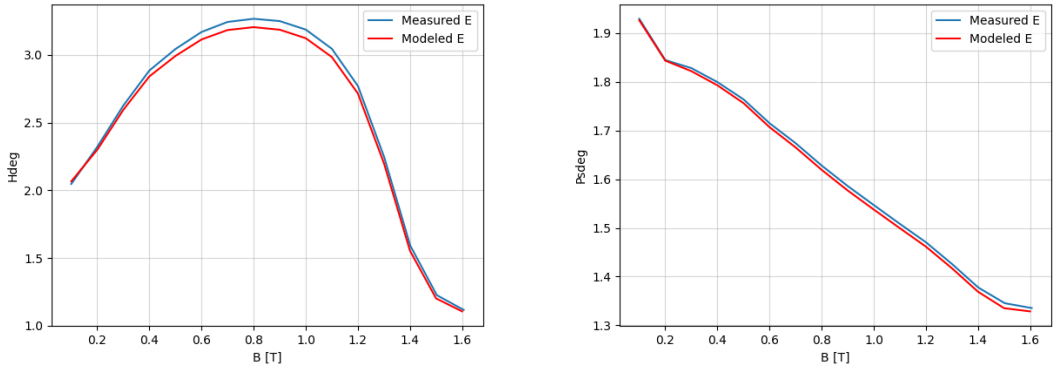

Figure 3.7: Modeled and measured H and P_s degradation for sample E at 200 Hz with sinusoidal feeding for laser cut NO25.

The obtained degradation models were used to get the BH and P_s curves for the material up to 1 mm from the cut edge which were then implemented in the degraded EM model. These curves as well as the measured curves for laser cut NO25 samples A-E at 200 Hz can be seen in Figure 3.8. The BH curve was used to define the degraded material in Ansys and the P_s curve was used to obtain the loss model coefficients.

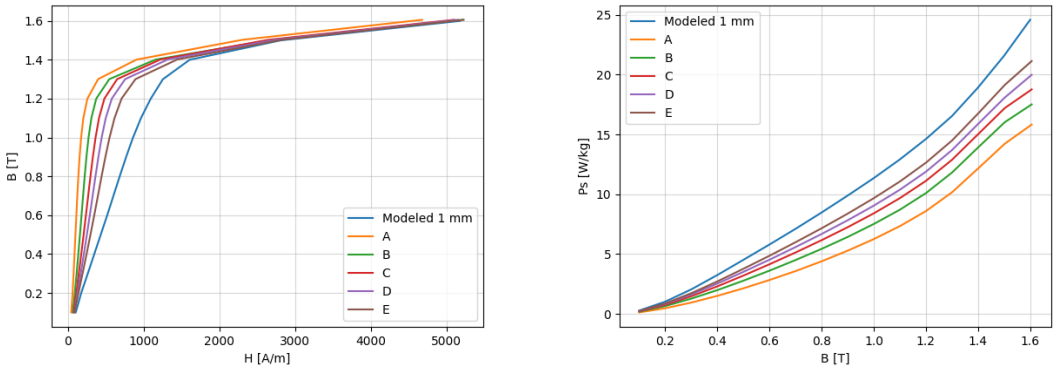

Figure 3.8: Measured BH and P_s curves for samples A-E and modeled BH and P_s at 1 mm from cut edge for 200 Hz for laser cut NO25.

3.2.2.1 Mesh

For the meshing of the EM model, length based refinement was used. The maximum element lengths for the different parts of the EM are presented in Table 3.11. These values were chosen since the mesh should be fine enough to give an accurate result but not too fine since that would significantly increase the computation time of the simulations. Furthermore, in order to increase the mesh density around the permanent magnets near the air gap two objects were added inside the rotor close to its outer edge. The resulting mesh can be seen in Figure 3.9.

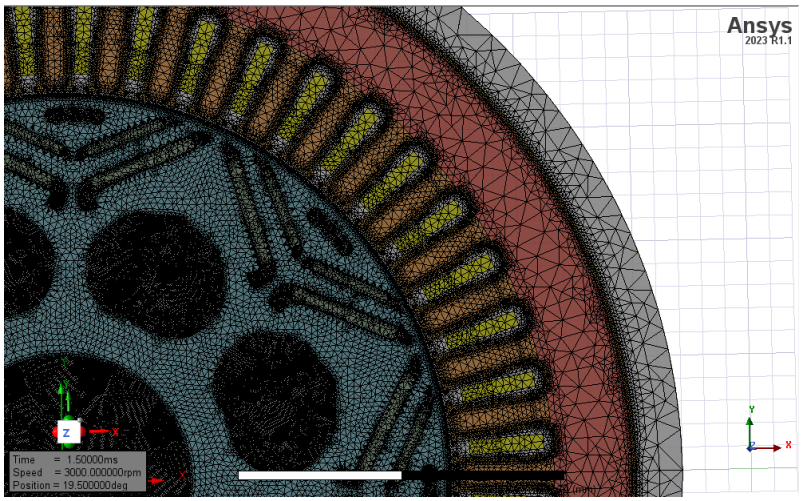

Figure 3.9: The mesh of the EM model.

Table 3.11: Maximum number of elements for the mesh of each part of the model.

Part	Maximum length of elements [mm]
Airgap	0.5
Coils	3
Magnets	2
Rotor	2
Rotor outer strips	1
Stator teeth	3
Stator yoke	5
Stator degradaded area	0.5

3.2.3 Loss Modelling

The Bertotti model was used to model the iron losses according to (2.2). This could be implemented in Ansys Maxwell by inserting the corresponding loss coefficients for each of the four materials used in the simulation. To have some physical meaning, k_{ec} was calculated using (2.3) and was the same for all four simulations. The other coefficients, k_h and k_{ex}, were obtained by curve-fitting the Bertotti model to the power loss curve for each of the cases so that there is one set of coefficients for each material. Further, one model is needed for each frequency to be studied. The Bertotti modeled and measured P_s curve for the non-degraded punched NO25 material at 200 Hz can be seen in Figure 3.10. The same procedure was done for the three remaining cases.

The resulting Bertotti coefficients for each of the materials for the simulations are presented in Table 3.12. Since the hysteresis and excess loss coefficients are modeled purely mathematically by curve-fitting, they have no physical meaning and thus no loss separation was done. The total iron losses are modeled with this method

but the proportions between the different types of losses are not modeled. These coefficients were then implemented in the simulations in Ansys Maxwell.

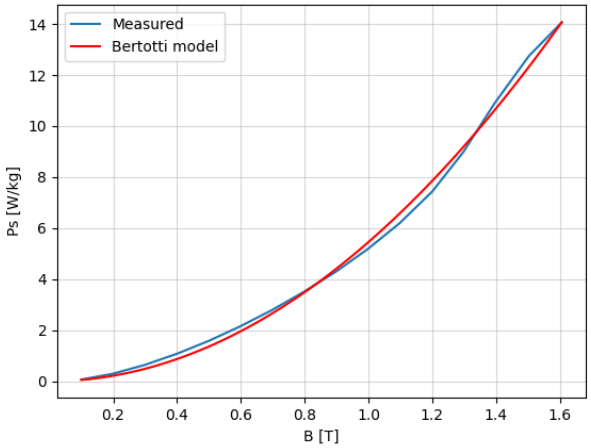

Figure 3.10: Measured and Bertotti modeled P_s for non-degraded punched NO25 at 200 Hz.

Table 3.12: The Bertotti coefficients used to model the iron losses.

Material	k_h	k_{ec}	k_{ex}
Non-degraded punched NO25	172.8	0.172	0
Degraded punched NO25	97.3	0.172	15.1
Non-degraded laser cut NO25	137.7	0.172	5.2
Degraded laser cut NO25	162.2	0.172	15.1

4

Measurement results

4.1 Repeatability test

In order to confirm that the same result is obtained each time a measurement is done, a repeatability test was performed. For this, the same measurement on sample A strips at 100 Hz and B-values from 0.1 to 1.9 T was done 20 times. Every fifth measurement, there was a pause of five minutes to let the equipment and steel strips rest. The percentage difference between different measurements and the mean value for each B-value can be seen in Figure 4.1.

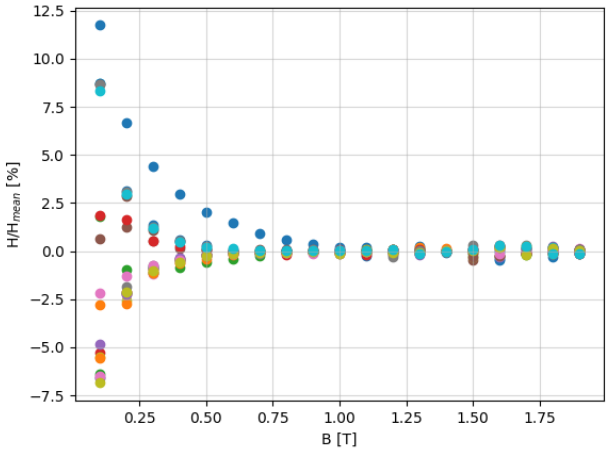

Figure 4.1: Repeatability test with punched NO25 sample A measured 20 times with the Epstein frame at 100 Hz with sinusoidal feeding.

From the figure, it can be seen that the largest difference occurs at the lowest B-values. At this point, the difference is up to 12 %. For the higher B-values, the difference is lower. This means that the results between different tests are fairly accurate but still vary some, especially at low B-values, which is good to keep in mind throughout this report.

4.1.1 Epstein frame vs SST

A comparison was made between measurements taken with the Epstein frame and the SST to see how they differ from each other. This H and P_s difference for measurements on sample A with the punched NO25 material at 100 Hz is presented in Figure 4.2. The largest difference in H between measurements taken with the SST and Epstein frame is around 7 % which occurs for B-values of 0.9-1.0 T. The

largest difference for the specific power loss is 10 % at $B = 1.7$ T. For most of the other measured values of B, the difference is a lot smaller. Since some samples in this thesis are measured with the Epstein frame and some with the SST, this difference should be kept in mind throughout the results.

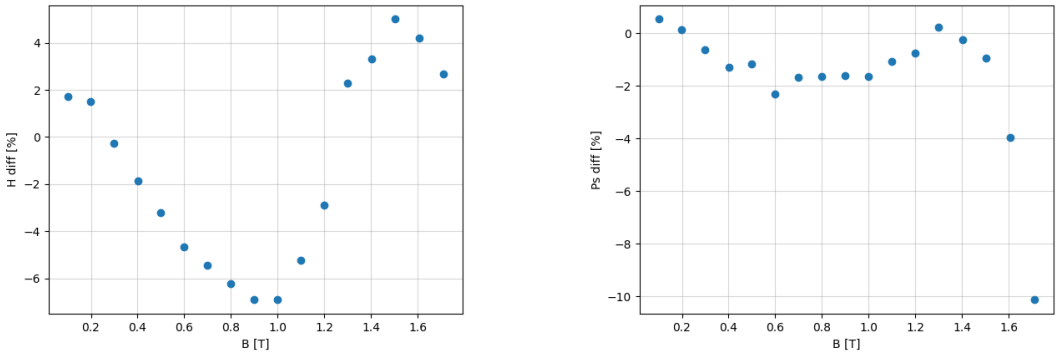

Figure 4.2: The difference between measurements of H and P_s taken with the Epstein frame and SST on punched NO25 sample A at 100 Hz.

4.1.2 Air flux compensation

When measuring using an Epstein frame, some flux in the air surrounding the electrical steel samples is also measured. This is not desired since only the flux in the steel should be considered. To compensate for this, a mutual inductor can be used in the measuring equipment. For the Epstein frames used in this thesis, only the 700 winding configuration has an option to use air flux compensation. In Figure 4.3, the magnetic field strength for measurements with and without air flux compensation and the difference between them is presented. It can be seen that the difference becomes very substantial between the two at higher flux densities especially. The largest difference occurs at the highest measured B-value where the difference is over 140 %. In this thesis, the Epstein frame 700 winding configuration with air flux compensation is not used and this large difference will thus not affect the comparisons in this particular investigation.

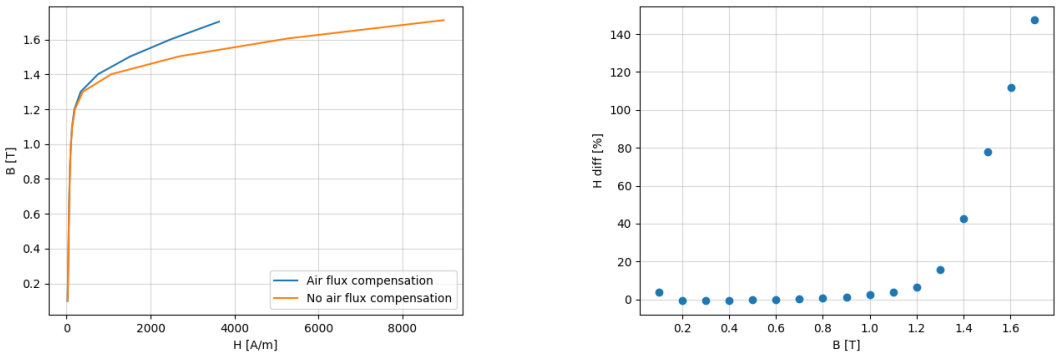

Figure 4.3: H and H_{diff} for measurements with the Epstein frame 700 winding with and without air flux compensation on punched NO25 sample A at 100 Hz.

4.2 Sinusoidal

The results from the sinusoidal measurements are presented in this section. At first, a comparison with the data sheet will be shown. Then the measured magnetic field strength and specific power loss for each sample will be visualised in different ways.

Sample A will be used as the non-degraded material and should therefore in an ideal world have the same behaviour as the data sheet for the material. In Figure 4.4, a comparison is made between the flux density and the magnetic field strength for sample A and the data sheet for four frequencies given in the data sheet. The measurements show that sample A needs a higher magnetic field strength to reach the same flux density as the data sheet does, indicating that it has some degradation.

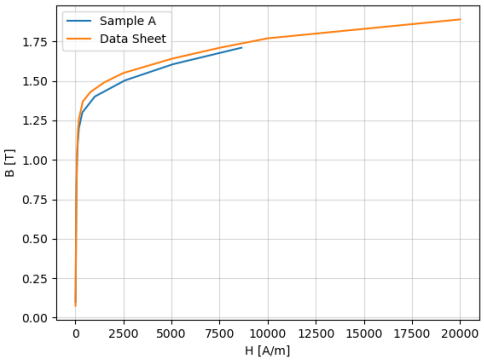

(a) 50 Hz

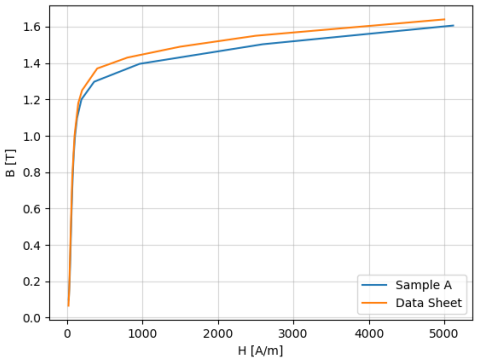

(b) 200 Hz

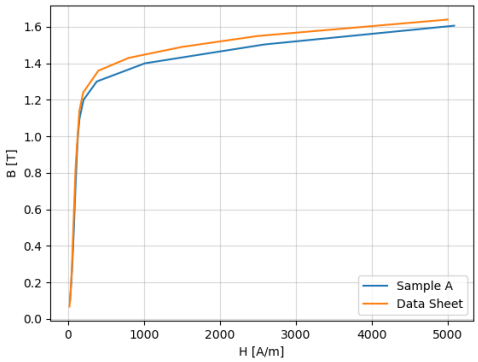

(c) 700 Hz

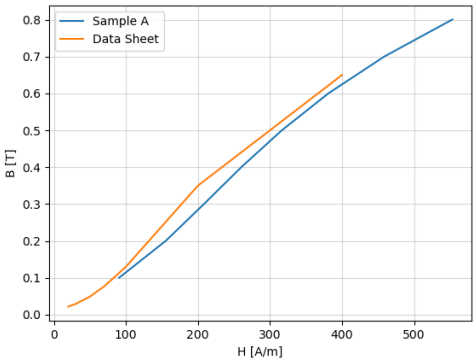

(d) 10 kHz

Figure 4.4: Comparison of BH-curves for measurements of NO25 punched and the data sheet.

Figure 4.5 shows a comparison of specific power loss and flux density between sample A and the data sheet. Overall, sample A has a slightly higher power loss than the data sheet. Sample A is not showing the exact same results as the data sheet but will be used as the non-degraded material throughout this thesis.

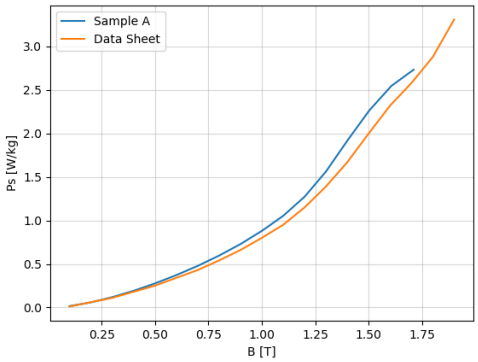

(a) 50 Hz

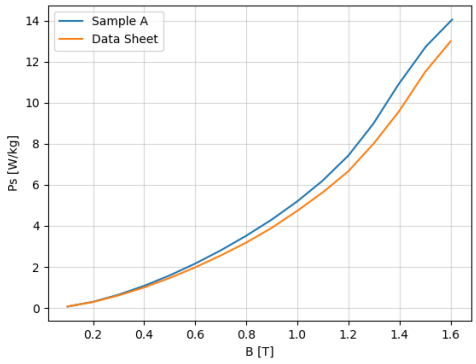

(b) 200 Hz

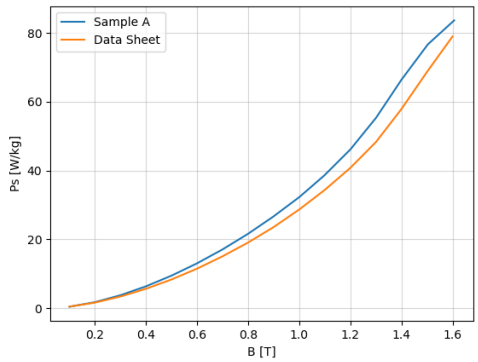

(c) 700 Hz

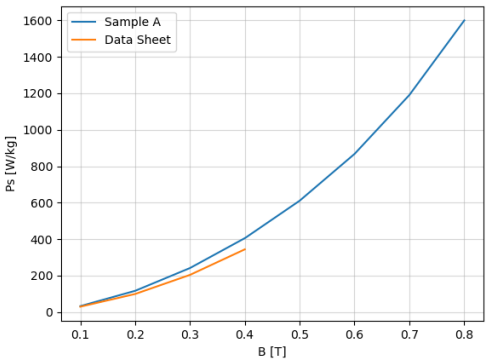

(d) 10 kHz

Figure 4.5: Comparison of power loss between measurements for NO25 punched and the data sheet.

The BH curves for each sample measured with sinusoidal feeding and a frequency of 200 Hz can be seen in Figure 4.6. The different samples have BH curves that differ from each other and it can be seen that the samples with more cuts require a higher magnetic field to reach the same flux density. As the distance to the cut edge decreases, a higher value of H is needed to obtain the same value of B. The figure only shows the BH curves at 200 Hz, but a similar behaviour is observed for each of the measured frequencies. To visualise the degradation effects more clearly, the degradation itself was plotted in Figure 4.6. The field strength degradation H_{deg} in this thesis is defined as

$$H_{deg} = \frac{H_x}{H_A} \tag{4.1}$$

where H_x is the value of the magnetic field strength for each sample. Thus, H_{deg} shows how much field strength that is required for a sample to reach a certain flux density compared to sample A. From Figure 4.6, it can be seen that the degradation varies with B-level and that the maximum degradation occurs around 1.2-1.3 T. The BH curves will be used as inputs for the material in the simulations in Ansys. The curve of sample A is used for the non-degraded model, while the other samples' curves are used to model the degradation.

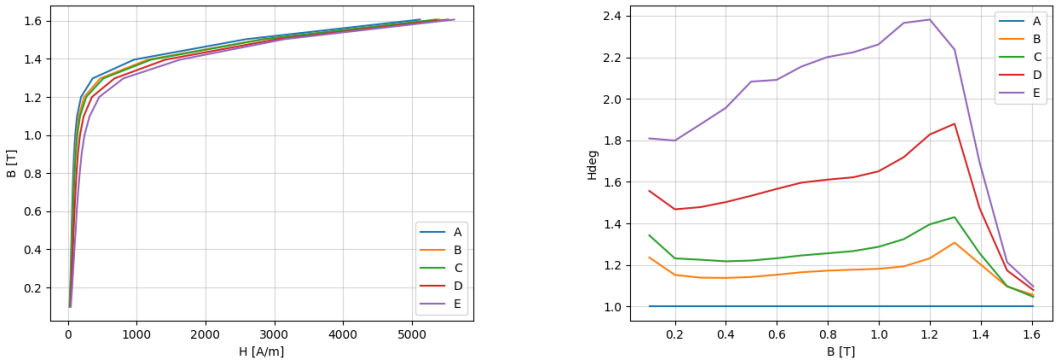

Figure 4.6: BH curves and field strength degradation for punched NO25 samples A-E at 200 Hz with sinusoidal feeding.

To study the degradation effect further, the field strength degradation was plotted against the distance from the cut edge in Figure 4.7. In order to do this, each sample was related to a distance from the cut edge which was done by dividing each width by two. So the distance from the cut edge for each sample is half of its width. This is an averaged value to that distance and not a simultaneous value, but the simplification makes it possible to visualise the degradation as in Figure 4.7. The simplification will be discussed in a later chapter. The figure shows that the degradation is the highest close to the cut edge and then it decreases as the distance from cut edge increases.

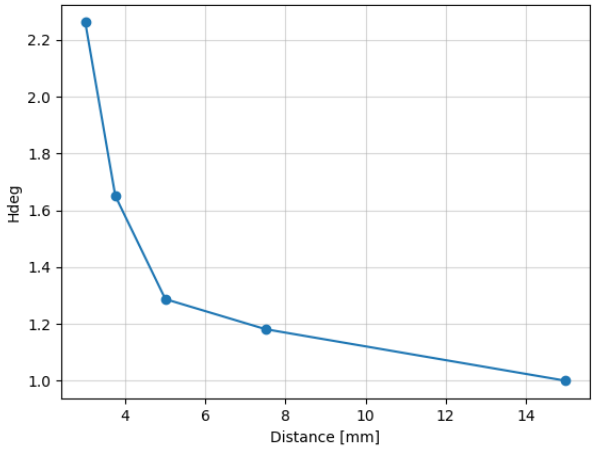

Figure 4.7: Field strength degradation vs distance to cut edge for punched NO25 at 200 Hz and $B = 1$ T with sinusoidal feeding.

Another parameter to consider is the relative permeability of the material. Each sample measured has a different permeability curve which can be seen in Figure 4.8. Sample A has the highest value and then as the width is decreasing, the permeability decreases which once again shows the degradation effect.

In Figure 4.8, the hysteresis loop for each sample can also be seen. The loop gets more tilted as the sample width is decreasing since more field strength is required to reach the flux density. Further, the area of the hysteresis loop is increased as the sample width is decreasing, so sample A has the smallest area while sample E has the largest area. The values of the areas can be found in Table 4.1. A larger area is an indication of higher hysteresis loss which also implicates the degradation effect for the samples.

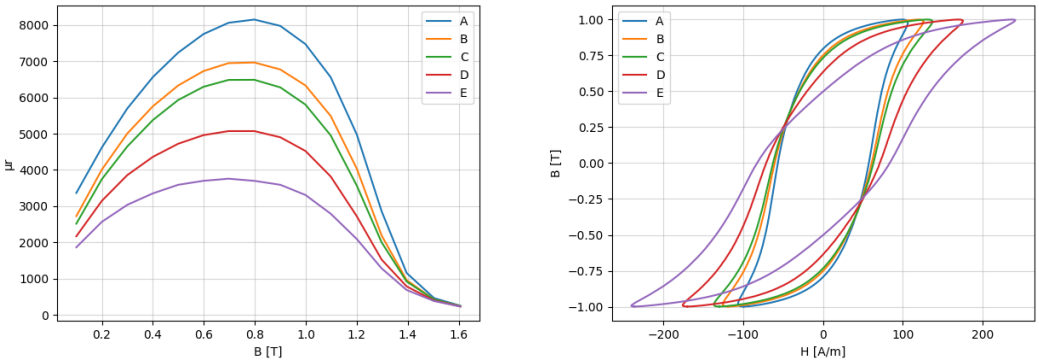

Figure 4.8: Permeability and hysteresis loops at $B = 1$ T for punched NO25 samples A-E at 200 Hz with sinusoidal feeding.

Table 4.1: Area of the hysteresis loop for samples A-E with punched NO25 at 200 Hz with sinusoidal feeding.

Sample	Area
A	156.1
B	167.1
C	177.4
D	191.7
E	213.8

The specific power loss was also measured and the resulting curve for each sample at 200 Hz is presented in Figure 4.9. It can be seen that the loss is higher for the samples with more cuts than for the ones with fewer cuts and as the distance to cut edge is decreasing, the loss is increasing. When modelling the iron losses using the Bertotti model, these power loss curves are used for curve fitting the coefficients. Similar to the field strength degradation, the specific power loss degradation, $P_{s,deg}$, was calculated according to

$$P_{s,deg} = \frac{P_{s,x}}{P_{s,A}} \tag{4.2}$$

The resulting degradation is presented in Figure 4.9. As the sample width decreases, the losses increase which can be seen clearly in the figure. For H_{deg}, there was a peak at 1.2 T which is not the case here. The power loss degradation is highest at the lowest flux densities and then decreases for higher values of B.

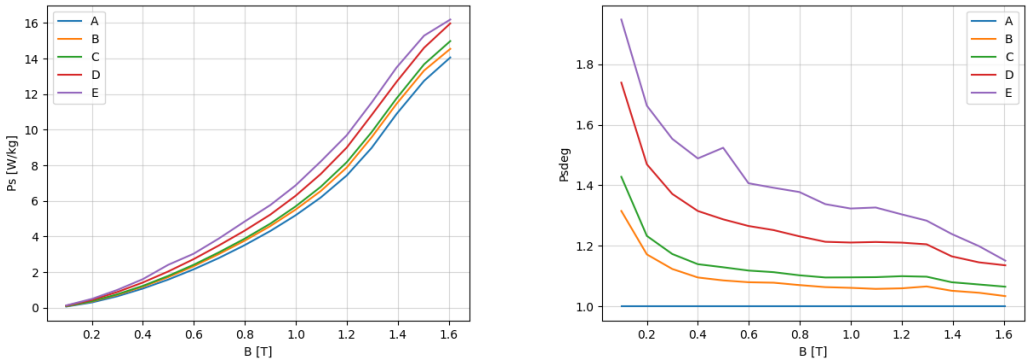

Figure 4.9: Specific power loss vs flux density and power loss degradation for punched NO25 samples A-E at 200 Hz with sinusoidal feeding.

The specific power loss degradation at each distance from the cut edge was determined in the same way as the field strength degradation and can be seen in Figure 4.10. The degradation is highest closer to the cut edge and decreases quite exponentially as the distance to cut edge increases.

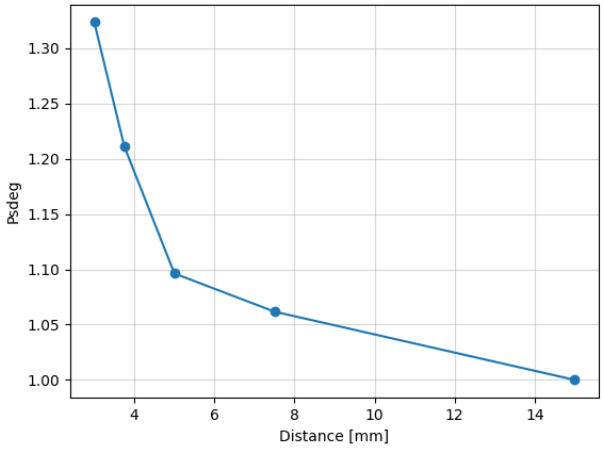

Figure 4.10: Power loss degradation vs distance to cut edge for punched NO25 at 200 Hz and $B = 1.0$ T with sinusoidal feeding.

4.3 Comparison with other materials

This section presents the results from measurements of six different sets of samples with different compositions of material, manufacturing method and thickness. The measurements were taken with sinusoidal feeding for frequencies of 200 Hz and 600 Hz, and the figures show the results for 200 Hz. Firstly, a comparison between punched and laser cut NO25 is made. Then, the difference between NO35 with different cut directions is studied and finally NO27_3 punched, NO35_1 punched, NO25_1 punched, NO25_1 laser cut and NO25_2 SOTA are compared.

4.3.1 Laser cut vs punched NO25

The measurements of punched and laser cut NO25 are compared to see what effects the different cutting techniques have on the same material. In Figure 4.11, the BH-curves of sample A for the punched and laser cut NO25 as well as the percentage difference between them is presented. A higher magnetic field strength is needed for the laser cut sample to reach the same flux density as the punched one for all B-levels except 1.3-1.6 T. It is uncertain if this is actually true or if it is a result of measurement uncertainties.

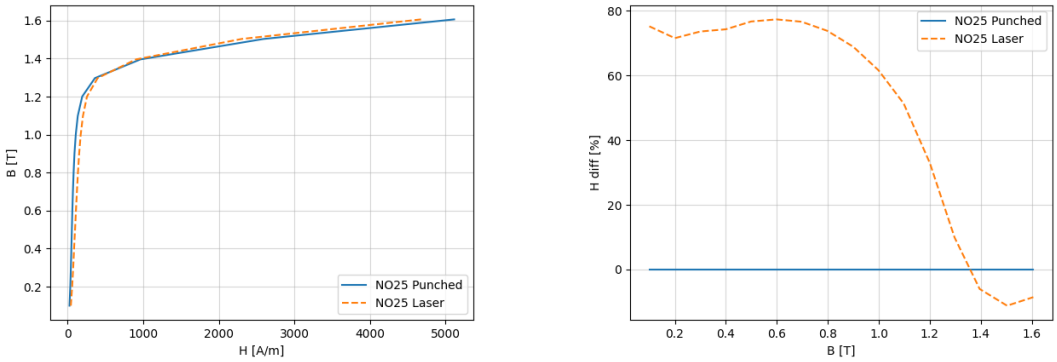

Figure 4.11: H vs B for sample A with punched and laser cut NO25 and the difference between them at 200 Hz with sinusoidal feeding.

The relative permeability of sample A with punched and laser cut NO25 was also compared which can be seen in Figure 4.12. It can be seen that μ_r is higher for the punched material than for the laser cut one which means that laser cutting seems to affect the material properties more than punching. It is also very apparent that the cutting method has an impact on the magnetic properties of the material.

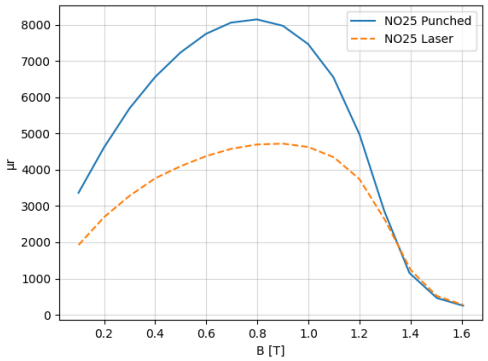

Figure 4.12: Relative permeability vs flux density of sample A with punched and laser cut NO25 at 200 Hz with sinusoidal feeding.

Figure 4.13 shows the specific power loss for sample A with punched and laser cut NO25 and the percentage difference between them. It can be seen that the loss is

higher for the laser cut sample for all measured B-values. At the lowest B, the difference is around 80 % and then it decreases to about 15 % at the highest values. This again shows that laser cutting seems to affect the material more than punching.

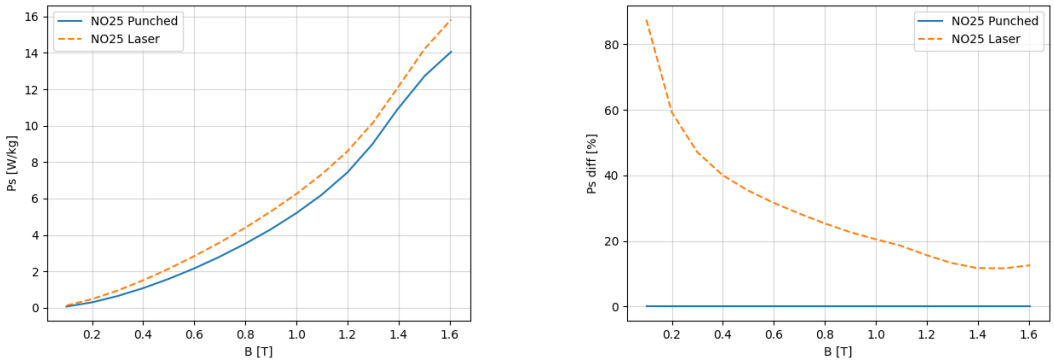

Figure 4.13: Power loss for sample A with punched and laser cut NO25 and the difference between them at 200 Hz with sinusoidal feeding.

Another factor to consider in this comparison is how the degradation is affected with the two different cutting methods. The H degradation for all sample types and the degradation against the distance to the cut edge are calculated as in the previous section and are presented in Figure 4.14. The laser cut samples have the laser cut sample A measurement as reference and the punched samples have the punched sample A measurement as reference. The plotted degradation against distance from the cut edge is at $B = 1$ T but the same behavior is seen at all measured B-levels. It can be seen in both figures that the degradation is higher for the laser cut samples than for the punched ones. Further, it can be seen that the H degradation seems to follow the shape of the permeability for the laser cut samples with a peak around $B = 0.8$ T while the punched samples do not follow this shape and have a maximum degradation around $B = 1.2$ T.

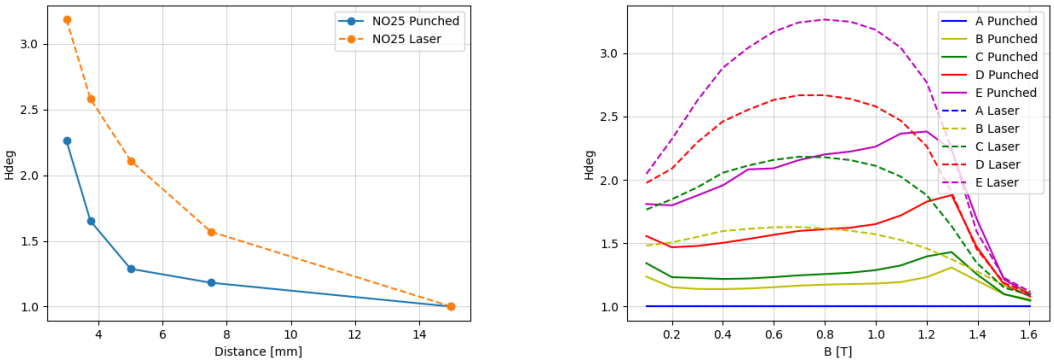

Figure 4.14: H degradation vs distance to cut edge at $B = 1$ T and H degradation for samples A-E for punched and laser cut NO25 at 200 Hz.

The power loss degradation for the punched and laser cut samples can be seen in Figure 4.15. The plot of degradation against distance from the cut edge is with $B = 1$ T but again, the same behavior can be seen for all measured levels of B. Similarly to the H degradation, it can be seen that the P_s degradation is higher for the laser cut samples than for the punched ones. It can also be seen in the figure to the right that the degradation varies more linearly with B for the laser cut samples than for the punched samples. As mentioned previously, these plots have been for measurements at 200 Hz but the same observations are made for the measurements at 600 Hz.

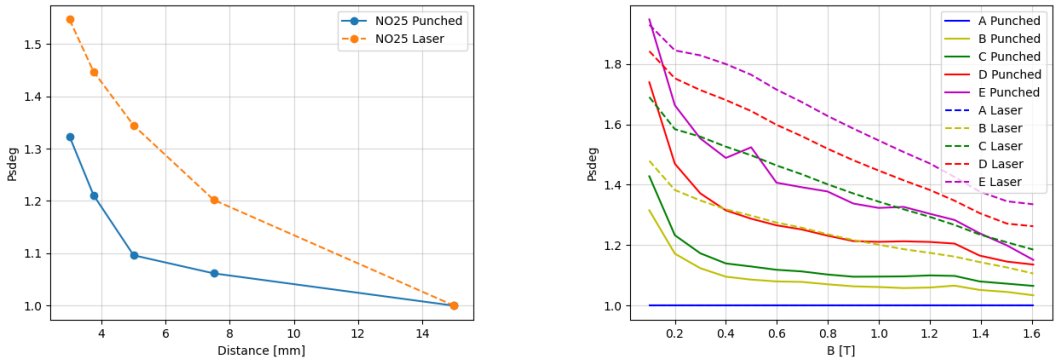

Figure 4.15: P_s degradation vs distance to cut edge at $B = 1$ T and P_s degradation for samples A-E for punched and laser cut NO25 at 200 Hz.

4.3.2 Cross vs length NO35

In this section, the degradation effects on samples cut in the cross and length direction will be compared. In Figure 4.16, the magnetic field strength is plotted against the flux density for NO35 sample A with both cutting directions and the difference between them is also presented. The sample that is cut in the length direction requires a lower H to reach the same B as the one cut in the cross direction for all values of B.

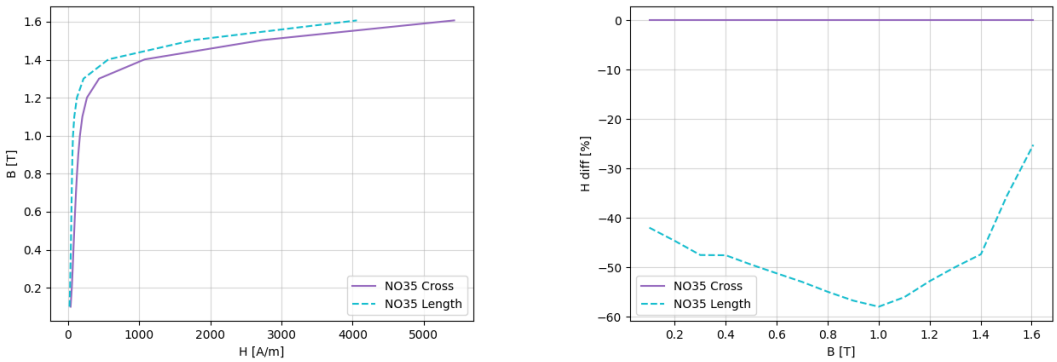

Figure 4.16: H vs B for sample A with NO35 cut in the cross and length direction and the difference between them at 200 Hz with sinusoidal feeding.

The relative permeability of NO35 sample A cut in the cross and length direction can be seen in Figure 4.17. The value of μ_r is higher for the sample cut in the length direction for all values of B which is to be expected from Figure 4.16. At the peak, the cross cut sample has a permeability that is more than 60 % lower than the length cut sample. This suggests that the direction that the material is cut in significantly affects the magnetic properties of the material.

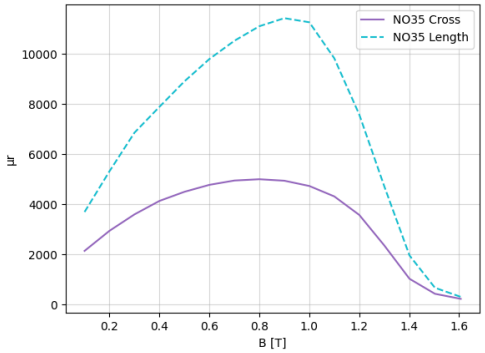

Figure 4.17: Relative permeability vs flux density of sample A with NO35 cut in the cross and length direction at 200 Hz with sinusoidal feeding.

In Figure 4.18, the specific power loss curves for NO35 sample A cut in both directions and the difference between them is presented. It can be seen that the loss is lower for the sample cut in the length direction for all B-values. The difference is the largest at low values of B and decreases as B increases. This shows, once again, that the material cut in the length direction has better magnetic properties than the one cut in the cross direction.

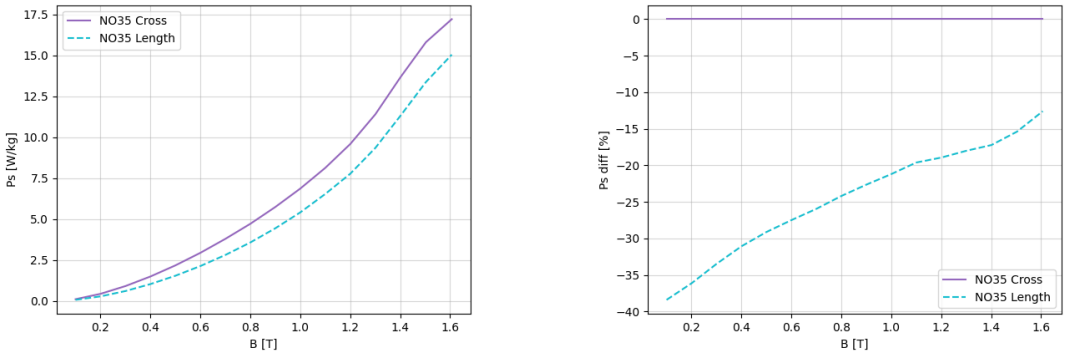

Figure 4.18: Power loss for sample A with NO35 cut in the cross and length direction and the difference between them at 200 Hz with sinusoidal feeding.

The field strength and power loss degradations were also compared for the two different cutting directions. This was calculated in the same way as preciously in the report and each sample has sample A cut in the same direction as its reference in order to look at the actual degradation. So the samples cut in the length direction are compared with sample A cut in the length direction and the samples cut in the cross direction are compared with sample A cut in the cross direction.

In Figure 4.19, the H and P_s degradation is plotted against distance from cut edge for both cutting directions at $B = 1$ T. For both the H and P_s degradation, the sample cut in the length direction has a higher degradation at all distances from the cut edge. From the previous figures, the sample cut in the length direction has better magnetic properties and less losses but in Figure 4.19, this sample has higher degradation. Therefore, even though it has better magnetic properties in general, it is important to consider the degradation since the most degraded sample could still have worse properties than the cross cut one.

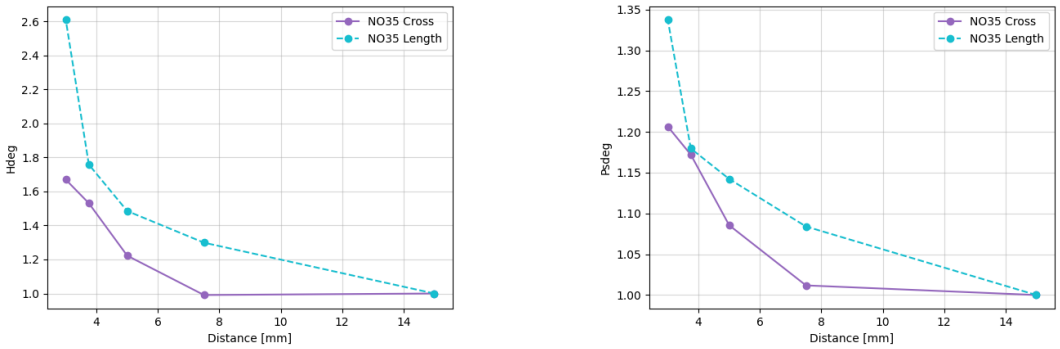

Figure 4.19: H and P_s degradation vs distance to cut edge at $B = 1$ T for NO35 cut in the cross and length direction at 200 Hz with sinusoidal feeding.

4.3.3 Material comparison

In this section the last number in the material name indicates the composition of silicon steel. For eaxmple, NO25_1 are made of the same material as NO35_1. Displayed in Figure 4.20 is the magnetic field strength for sample A for each material as well as the percentage difference in field strength for each material compared to the punched NO25_1 material. The results vary depending on B but it is clear that NO27_3 punched always needs a lower H to reach the same flux density compared to the rest of the materials. It is also notable that compared to the other materials, NO25_1 punched shows a change in behaviour at around 1.1-1.3 T.

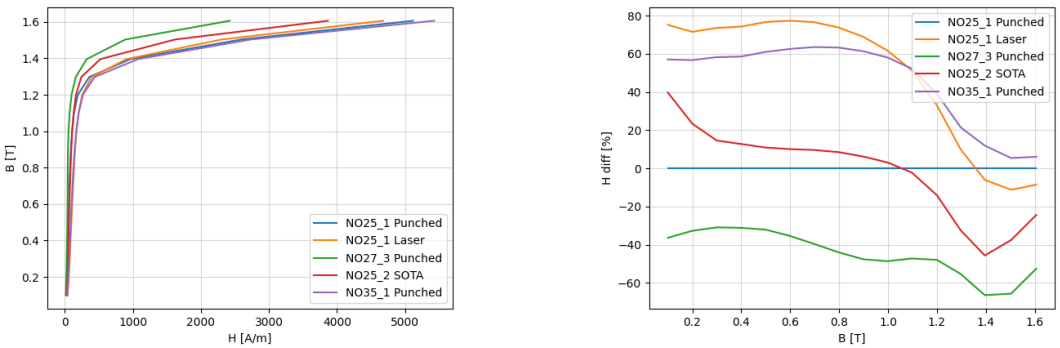

Figure 4.20: H vs B for sample A with different materials and the difference between them at 200 Hz with sinusoidal feeding.

In Figure 4.21, the permeability for each material is presented. There is a relation between the field strength and the permeability and it is apparent that NO27_3 punched has the highest permeability. From the previous section, materials that have been cut in the length direction has better magnetic properties than ones that have been cut in the cross direction. The NO27_3 punched steel has been cut in the length direction while all other materials in the comparison in this section have been cut in the cross direction which is good to keep in mind. When looking at NO25_1 punched and NO35_1 punched, the thinner material, NO25, has a higher permeability. When comparing the two laser cut NO25 samples, it can be seen that the state of the art laser cut material has a higher permeability than the other one which is expected since the SOTA laser is meant to cut laminates for EMs while the industrial laser is not.

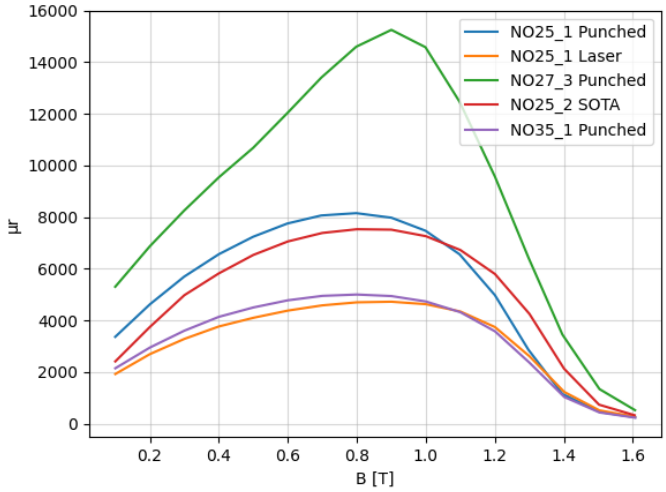

Figure 4.21: Relative permeability vs flux density of sample A with different materials at 200 Hz with sinusoidal feeding.

As expected from the two previous figures, NO27_3 punched has the lowest power loss. This can be seen in the Figure 4.22 where the power loss for each material as well as the difference in power loss compared to punched NO25 are plotted. Over all, similar behaviour can bee seen in the difference in power loss as in the difference in field strength. The difference between the materials is however not as big for the power losses. NO27_3 punched has the lowest power loss at all flux densities but regarding the other materials it varies depending on the flux density. The thicker NO35_1 punched has higher losses than the punched NO25 and NO25_2 SOTA has lower losses than the other laser cut material, NO25_1 laser.

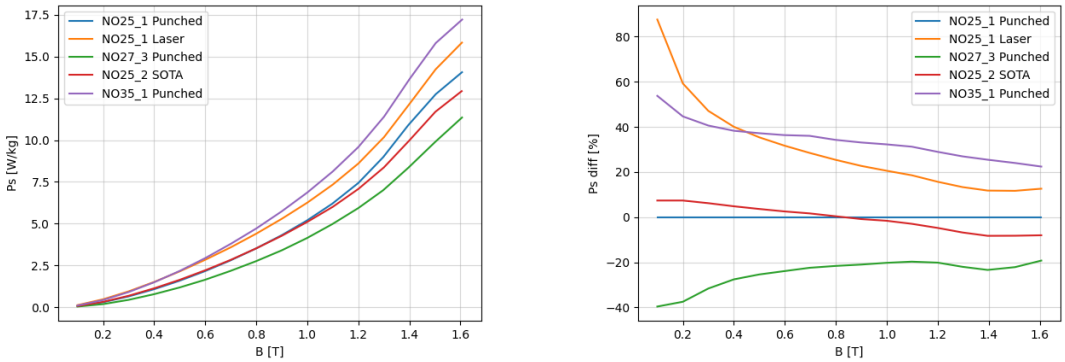

Figure 4.22: Power loss for sample A with different materials and the difference between them at 200 Hz with sinusoidal feeding.

In Figure 4.23, the H and P_s degradation at $B = 1$ T is plotted against the distance from the cut edge. The two laser cut samples have the highest value of degradation with NO25_2 SOTA having the most degradation. The degradation effects on the punched materials are lower with the thicker NO35_1 punched having the least degradation at all distances from cut edge. The degradation of NO27_3 punched steel is quite high close to the cut edge but has a steep decrease, so it quickly decreases as the distance is increasing.

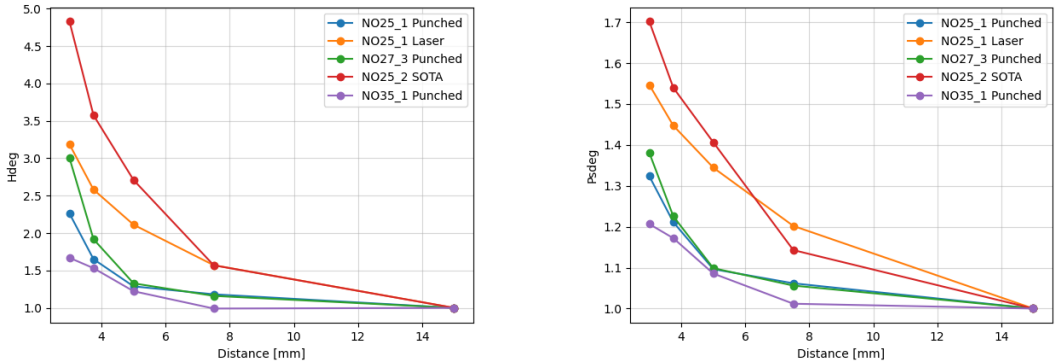

Figure 4.23: H and P_s degradation vs distance to cut edge at $B = 1$ T for different materials at 200 Hz with sinusoidal feeding.

As mentioned earlier, the thicker material, NO35_1 punched, has the highest specific power loss and the lowest permeability, but from Figure 4.23, it can be seen that NO35 has the lowest degradation. The thicker material has a lower permeability but is less affected by the degradation from cutting of the material. Figure 4.24 shows the power loss curve for each material of the sample E type. Since sample E is the most degraded sample, with the smallest width, comparing these will show how the losses differ between the degraded materials. This is interesting since some materials have higher losses than others but are less affected by degradation and the other way around. In the figure, it can be seen that NO25_1 laser has the highest loss for most values of B, while the NO35 material has the highest loss in Figure

4.22. In the same way, the degraded NO25_2 SOTA sample has higher losses than the degraded punched NO25 but the non-degraded NO25_2 SOTA has lower losses than the non-degraded NO25 for high B-values. NO27_3 punched has the lowest losses in both cases.

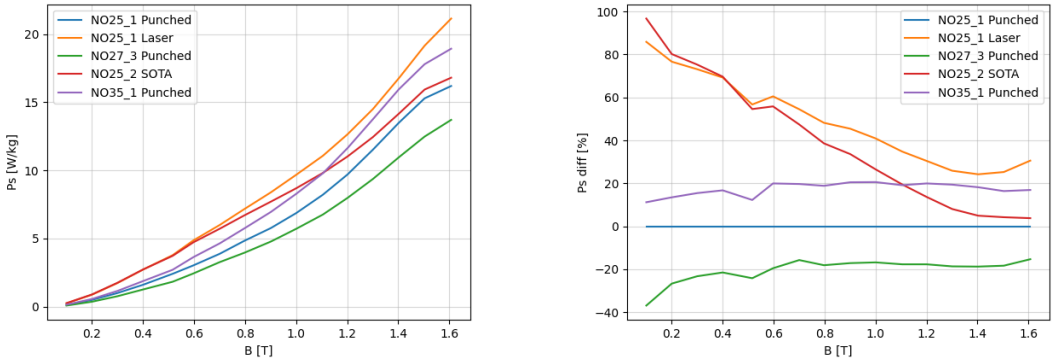

Figure 4.24: P_s vs B for sample E with each material and the difference from punched NO25.

4.4 PWM Excitation

This section presents the results from the PWM measurements. The PWM measurements were carried out in three parts, first is the results of how different values for the frequency modulation ratio f_r and the modulation index m_a affect the measurements. Then, from that result, specific values for f_r and m_a were chosen and the results for the degradation are presented.

4.4.1 Comparing frequency modulation ratio, f_r

In this section five different frequency ratios are compared, f_r=9, 11, 15, 99 and 199. When looking at the effect of different f_r, various m_a have been observed, the figures in this section will however present the results for m_r=0.3. The fundamental frequency for the measurements is 50 Hz and the results are therefore also compared to the 50 Hz measurement with sinusoidal feeding.

Figure 4.25 shows B, H, current and voltage vs time for one period. The measurements are done so that the same peak flux density of the fundamental curve is obtained for each f_r for comparability. The sinusoidal measurements are measured on the 700 turns Epstein frame while the PWM measurements are taken on the 60 turn Epstein frame. Therefore, the current and voltage for sinusoidal feeding are normalized to compensate for that difference. The voltage peak for sinusoidal feeding is one-third of the PWM measurements which is reasonable since m_a=0.3. It can clearly be observed that PWM feeding gives rise to ripple in B and H, where the ripple is highest for a lower frequency modulation index. The ripple is also significantly higher for H than for B, and this ripple will impact the power losses.

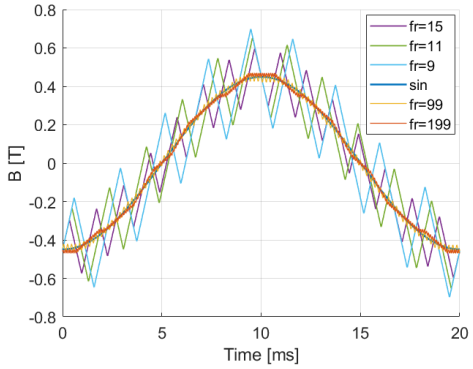

(a) B vs time

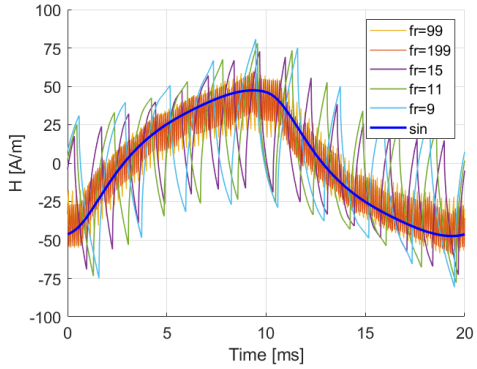

(b) H vs time

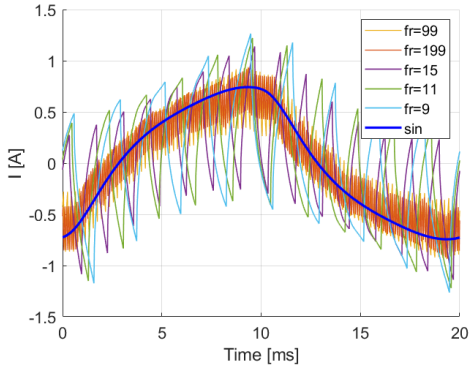

(c) Current vs time

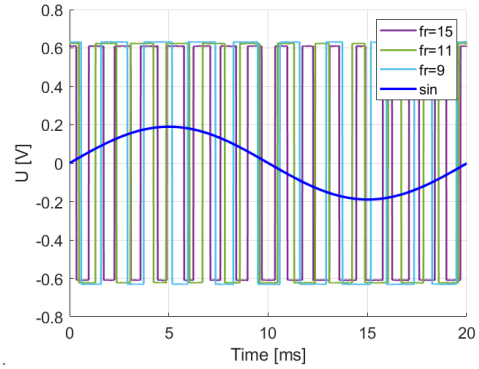

(d) Voltage vs time for f_r=9, 11 and 15

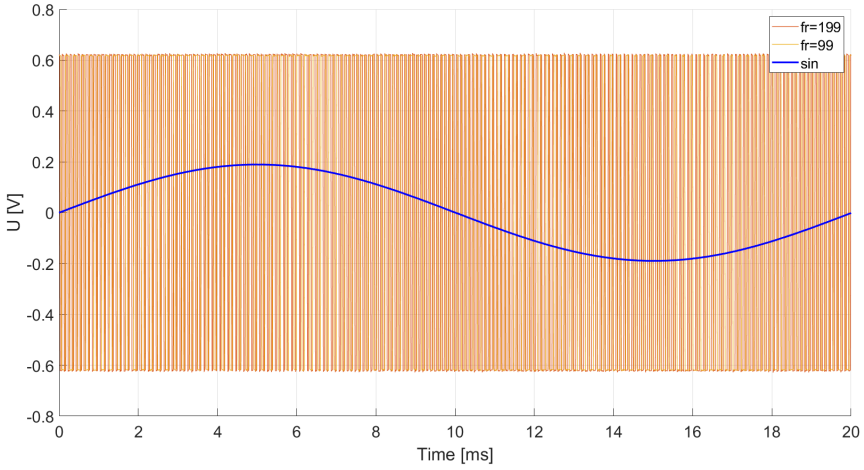

(e) Voltage vs time for f_r=99 and 199

Figure 4.25: B, H, current and voltage for one period for NO25 punched at m_a=0.3 and fundamental frequency 50 Hz and B=0.45 T. Sinusoidal current and voltage are normalized to compensate for different winding configurations in measurements.

The B-ripple seen at the peak in Figure 4.25a is presented in Table 4.2. When analyzing the ripple over all B-levels it can be seen that it increases linearly with the flux density and that the relation between different f_r are proportional. It is therefore possible to use one f_r as the reference and find a constant for each other f_r to make sure that they get the same peak of the fundamental flux density. Since the fundamental curve will appear at the middle of the ripple at the peak, the compensation constant should be proportional to half of the ripple.

Table 4.2: B-ripple at the peak for B=0.45 T

f_r	Ripple [T]
9	1.72
11	1.63
15	1.44
99	0.61
199	0.43

The most apparent difference between the sinusoidal feeding and PWM feeding can clearly be seen in the hysteresis loop in Figure 4.26 where each of the frequency modulation ratios are plotted together with the sinusoidal feeding. For the PWM feeding, minor loops within the big hysteresis loop can be observed. These loops occur due to the on and off switching of the magnetic field that is introduced by the PWM feeding. The big hysteresis loop results from a lagging between the increasing magnetic field and the flux density, and vice versa when the magnetic field is decreasing. The exact same thing happens with PWM feeding for each switching and it can be noted that f_r=9 gives rise to a total of 9 loops, f_r=11 gives rise to a total of 11 loops and so on.

The frequency ratio also affects the area of the minor loops, from Figure 4.26 it can be seen that the area for each minor loop decreases as f_r increases. This occurs since for higher f_r, the switching happens faster and the change of the magnetic field during each switching will be lower and therefore giving rise to a smaller area. The results in the hysteresis loops origin from the behaviour observed from the ripple for B and H in Figure 4.25. It can also be observed that the peak in B and H are higher for lower f_r which also can be seen in the big hysteresis loop.

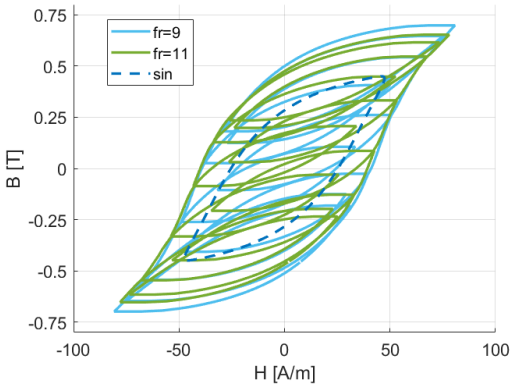

(a) Hysteresis loop for f_r=9 and 11

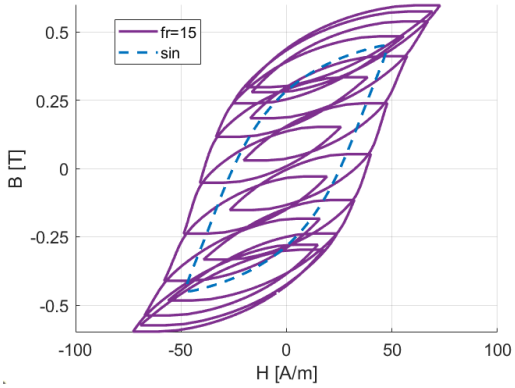

(b) Hysteresis loop for f_r=15

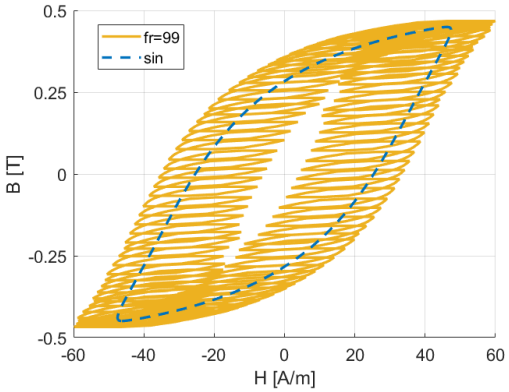

(c) Hysteresis loop for f_r=99

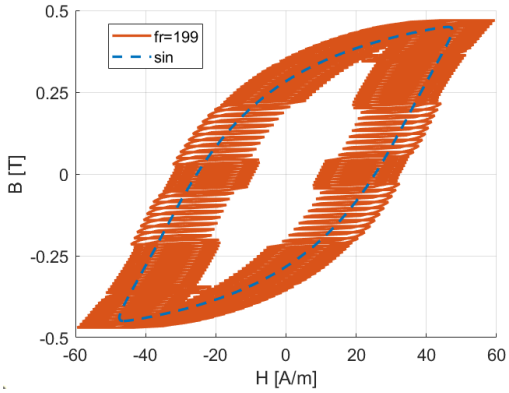

(d) Hysteresis loop for f_r=199

Figure 4.26: Hysteresis curves for NO25 punched at m_a=0.3 and fundamental frequency 50 Hz and B=0.45 T for five different f_r and for 50 Hz with sinusoidal feeding.

When looking at the core loss that appears, the two most important components are the B-magnitude and the frequency, since the iron loss is modeled according to (2.2). It is therefore interesting to look at the FFT of the flux density in Figure 4.27. The figure shows the total FFT as well as three zoomed in figures focusing on three different frequencies. First is the fundamental frequency, then the switching frequency for the lower f_r=9, 11 and 15 and at last the switching frequency for f_r=99 and 199.

It can be observed that the sinusoidal feeding only gives rise to a peak at the fundamental frequency, while the PWM feeding gives rise to several harmonics such as the biggest one at each switching frequency and also at multiples of the switching frequency ± the fundamental frequency. It can be seen that for higher frequency the peak becomes lower.

The peaks at the higher frequencies become important even if they are small since the eddy current loss is proportional to the squared frequency. The eddy current loss is more dominant for higher frequencies and the hysteresis loss are more dominant for lower frequencies since the hysteresis loss is only proportional directly to the frequency.

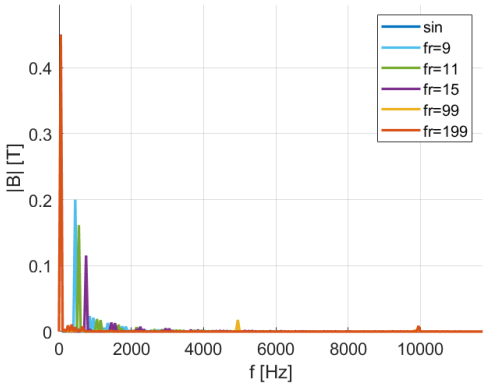

(a) Overview of the FFT

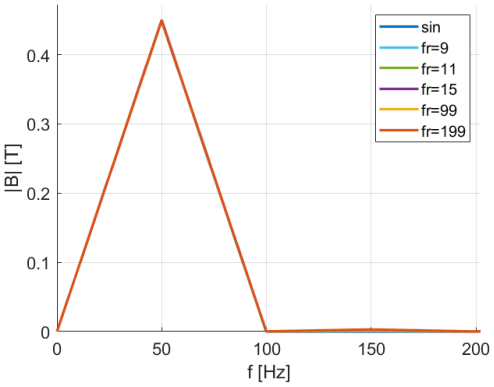

(b) FFT zoomed at the fundamental frequency

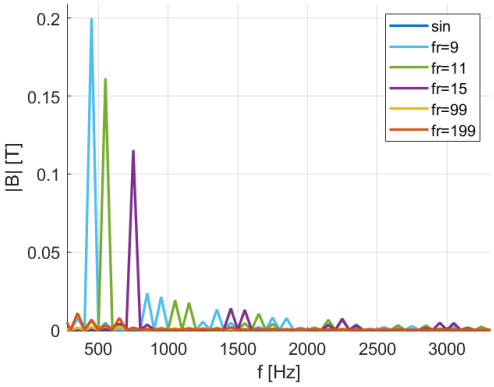

(c) FFT zoomed at low switching frequencies

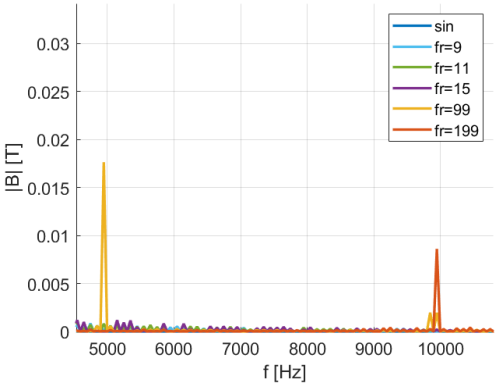

(d) FFT zoomed at high switching frequency

Figure 4.27: FFT on the flux density for NO25 punched at m_a=0.3, fundamental frequency 50 Hz and B=0.45 T for five different f_r.

The area from the hysteresis loops corresponds to the hysteresis loss and from Figure 4.26 the area increases for decreasing f_r. The same behaviour can also be seen in Figure 4.28 where the total loss is presented for all f_r and sinusoidal feeding. An evaluation is done to recreate the PWM losses with sinusoidal measurement values and are presented with dashed lines in Figure 4.28. It looks at the FFT and adds the power loss for the harmonic components. Table 4.3 presents how many harmonics that were included in the recreation for each f_r. The plot to the right shows the power loss difference in percentage for each f_r compared to the sinusoidal feeding in solid lines as well as the difference between each f_r and its recreated power loss in dashed lines.

Table 4.3: Number of harmonics included in the recreation of the power losses for each frequency modulation ratio.

f_r	Number of Harmonics
9	6
11	6
15	6
99	3
199	1

It is clear that for higher f_r the loss reduces significantly which is a result of much lower ripple in B and H compared to lower f_r. These results show that there is a substantial difference in the power losses between sinusoidal feeding and PWM. From literature it is indicated that the difference in iron loss in the EM can be up to 30 % which makes these results unexpectedly high. It is note worthy that the recreation does not reach as high losses as the PWM does. However, only a few harmonics could be added. The difference in loss between the recreated and PWM measurement ranges from 5 % at low flux densities to 60 % for high flux densities. But the difference is much higher for f_r=99 and 199, for the lower frequency modulation index the difference is never higher than 34 %.

The most realistic f_r for a vehicle implementation would be to have a high constant switching frequency, which in this case would correspond to f_r=199 and a switching frequency of 10 kHz. But for easier interpretations of the results, especially for the hysteresis loops, f_r=9 will be further evaluated regarding the degradation for PWM feeding.

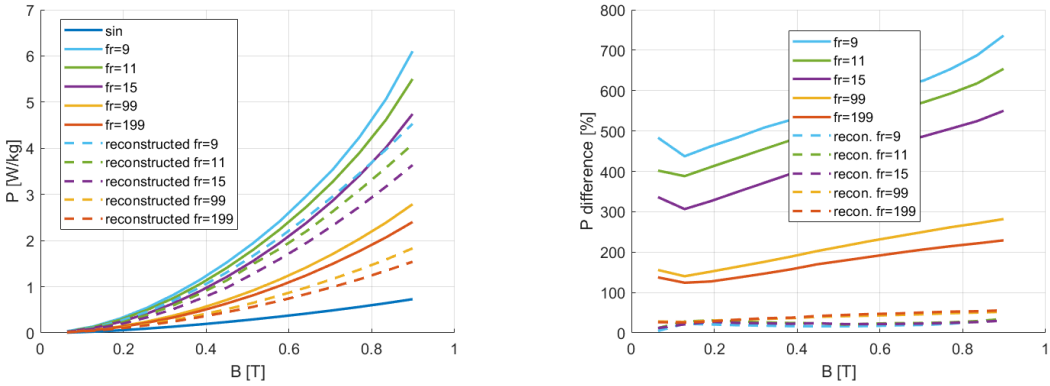

(a) Power loss **(b)** Power loss difference

Figure 4.28: Power loss and power loss difference for NO25 punched using sinusoidal feeding as the reference for f_r=9, 11, 15, 99 and 199.

4.4.2 Comparing modulation index m_a

This section compares how different modulation index affect the power losses. The modulation indices under observation are m_a=0.3, 0.4 and 0.5 with the frequency ratio set to f_r=9 and the fundamental frequency 50 Hz.

Looking at the hysteresis loops in Figure 4.29 where m_a=0.4 is first compared to m_a=0.3 and then compared to m_a=0.5 it can be observed that the lower value of the modulation index has a slightly larger area. The same behaviour can also be seen regarding the minor loops within the big hysteresis loop, lower values of m_a results in larger area.

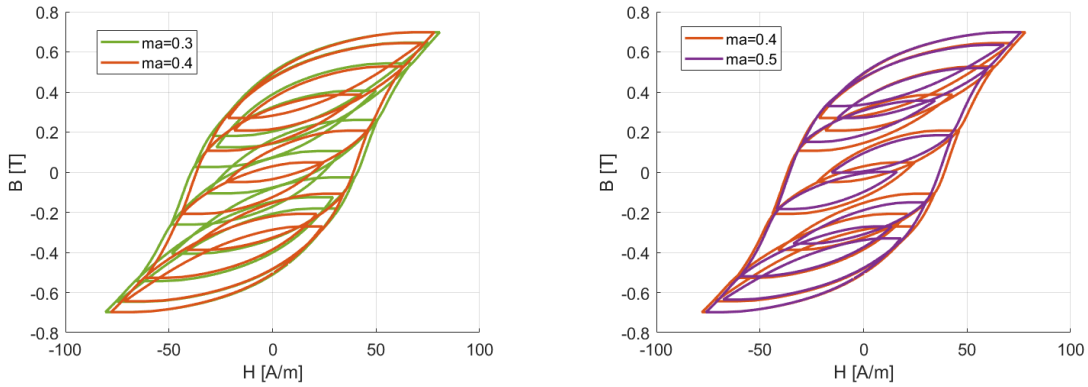

(a) Hysteresis loop for m_a=0.3 and 0.4 **(b)** Hysteresis loop for m_a=0.4 and 0.5

Figure 4.29: Hysteresis loops for NO25 punched with f_r=9 at fundamental frequency of 50 Hz and at B=0.45 T for m_a=0.3, 0.4 and 0.5

Since all of the measurements in the comparison have the same frequency ratio, it can be expected that all of them have the same frequency components. This can be verified in Figure 4.30 which plot the FFT of the flux density. It can be observed that the harmonics appear at the same frequencies but that the different modulation indices give rise to different magnitudes. It can be seen that the highest modulation index m_a=0.5 has the highest peak at the fundamental frequency and consequently lowest at the switching frequency. This highly affects the power losses since it is highly dependent on the frequency, and a low peak at higher frequency will reduce the total loss.

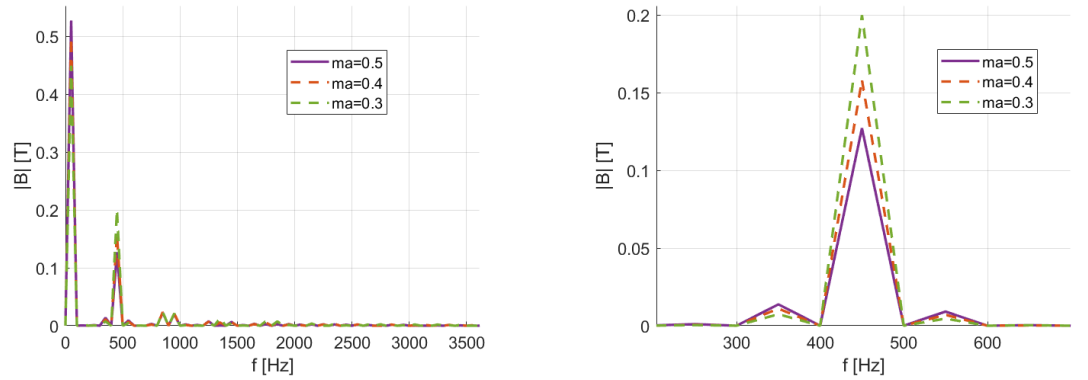

(a) FFT at fundamental frequency **(b)** FFT zoomed at switching frequency

Figure 4.30: FFT on the flux density for NO25 punched with f_r=9 with fundamental frequency of 50 Hz and at B=0.45 T for m_a=0.3, 0.4 and 0.5

Figure 4.31 presents the power loss for m_a=0.3, 0.4, and 0.5 as well as for sinusoidal feeding at 50 Hz. It also shows the difference in power loss for each modulation index compared to the sinusoidal measurement. As interpreted from the FFT it is clear that the higher m_a=0.5 has the lowest losses, then m_a=0.4 and at last m_a=0.3 has the absolute highest losses. The behaviour is clear over all flux densities as well. This indicates that using the lowest possible dc-link voltage is always faworable.

The modulation index has a great impact on the power losses for PWM feeding. A higher value of m_a results in lower losses but that is not what the EM in a vehicle application is experiencing since the modulation index varies with the speed and load of the operation. The most realistic value according to Figure 3.3 would be m_a=0.2 but this was not possible to obtain with the measurement equipment. Therefore, m_a=0.3 will be the modulation index that is observed further for the degradation due to PWM feeding.

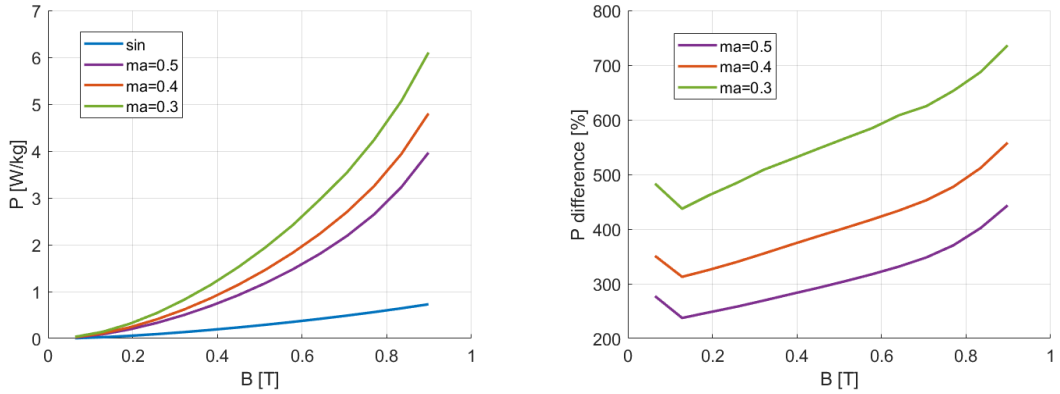

(a) Power loss **(b)** Power loss difference

Figure 4.31: Power loss and power loss difference for NO25 punched with f_r=9 using sinusoidal feeding at 50 Hz as reference for m_a=0.3, 0.4 and 0.5

4.4.3 Degradation

This section shows the results of the degradation effect on the power loss due to PWM feeding. In this section the frequency ratio is set to f_r=9, modulation index is set to m_a=0.3 and fundamental frequency will be 50 Hz. The results are also compared to degradation for sinusoidal feeding with a frequency of 50 Hz.

In Figure 4.32 the hysteresis loops for sample A and sample E are plotted both for PWM feeding and sinusoidal feeding. It is apparent that sample E is experiencing degradation for both the sinusoidal and PWM case. It can also be observed that degradation for PWM feeding is appearing in a similar way as for the sinusoidal feeding. The loops for sample E are more tilted than sample A and the area of the main hysteresis loop is bigger for sample A than for sample E in both cases. The tilting implicates that there is a degradation in magnetic field strength while the larger area is a implication of higher power loss. Looking closely at the minor loops for the PWM measurements it can be observed that also these have a higher area for sample E than for sample A.

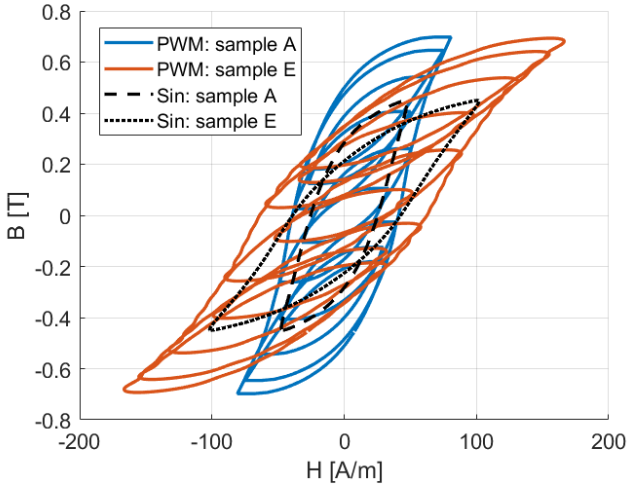

Figure 4.32: Hysteresis loops for NO25 punched with PWM feeding at fundamental frequency of 50 Hz, f_r=9, m_a=0.3 and sinusoidal feeding with 50 Hz at B=0.45 T, both for sample A and E.

The power loss can be seen in Figure 4.33, to the left is sample A and E for PWM and sinusoidal feeding while to the right all samples are included. It is apparent that the interpretation stated when looking at the hysteresis loops, that sample E have highest losses, is correct.

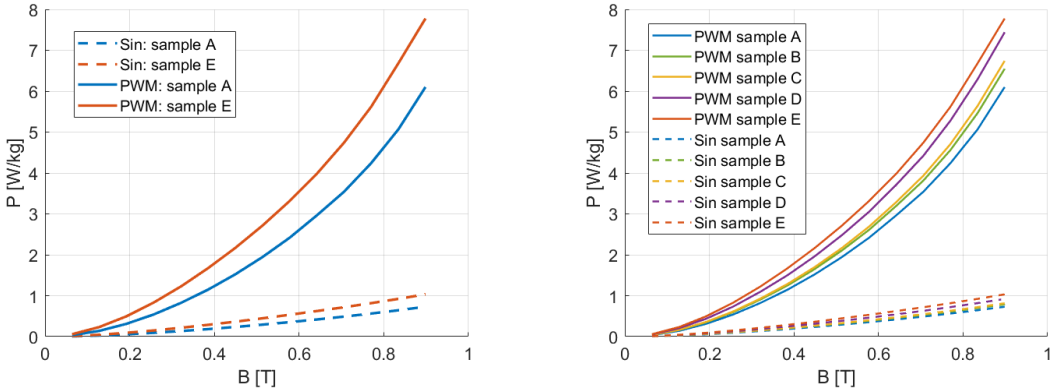

(a) Power loss for sample A and E

(b) Power loss for all samples

Figure 4.33: Power loss for NO25 punched with PWM feeding at fundamental frequency of 50 Hz, f_r=9 and m_a=0.3, sinusoidal feeding at 50 Hz.

Looking further into the degradation, two comparisons have been made for PWM feeding. Firstly, the degradation of PWM is obtained using sample A with PWM feeding as the reference. Then for the second case, the degradation is obtained using sample A with sinusoidal feeding as the reference. The results from both these degradation models as well as the results from sinusoidal degradation are presented in Figure 4.34. The plot to the right show the degradation as a function of distance

to the cut edge at B=0.45 T for the same three cases: PWM with PWM as reference, PWM with sinusoidal as reference and sinusoidal with sinusoidal as reference.

The degradation results show that the degradation for PWM feeding is appearing in a very similar way as the degradation with sinusoidal feeding. There is a substantial difference between the two feedings which become apparent when looking at the degradation for PWM feeding obtained with sinusoidal feeding as the reference. But since the degradation appears the same way for PWM feeding as for sinusoidal feeding, it can be concluded that the main difference appear due to the extra losses introduced by the extra harmonics from the PWM feeding and it does not appear to have any extra effect on the degradation. If anything, the degradation seem to be a bit lower for PWM feeding at 3 mm from the cut edge than for sinusoidal degradation.

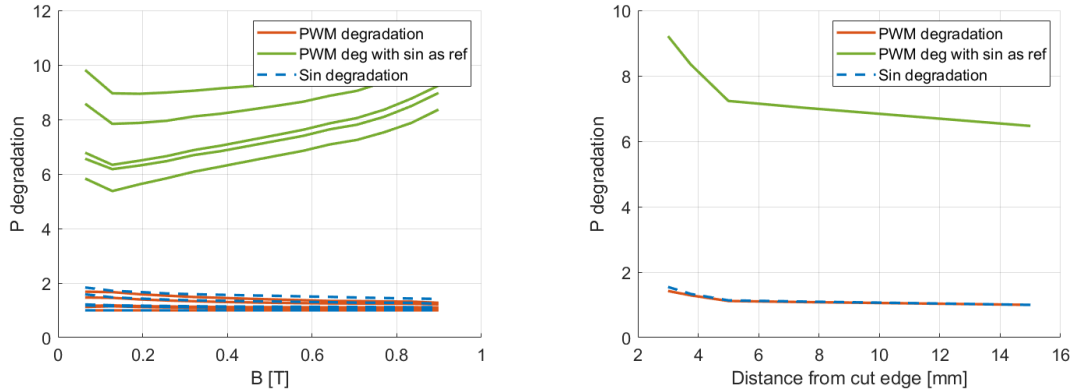

(a) Power loss degradation vs. B

(b) Power loss degradation vs. distance to cut edge at B=0.45 T

Figure 4.34: Power loss degradation vs B and distance from cut edge for NO25 punched.

5

Simulation results

In this section, the results from the FEM simulations of the EM with sinusoidal feeding will be presented. Four different simulations were done, with non-degraded punched NO25, degraded punched NO25, non-degraded laser cut NO25 and degraded laser cut NO25. The iron losses and efficiency will be compared for the degraded and non-degraded simulations to see how the EM is affected by the degradation of the material. Further, the results from the simulations with punched and laser cut NO25 will be compared.

For each of the simulations, a mapping was done to get an overview of how the EM is behaving throughout the whole operating range. The simulation was done at 200 Hz for currents between 0 and 500 A and then values were interpolated to create a torque speed map. Some of the results from the mapping of the EM with non-degraded punched NO25 can be seen below. Figure 5.1 shows the total losses and the total iron losses at each point and Figure 5.2 shows the transmitted power as well as the efficiency. It can be seen that the maximum torque is 420 Nm and that the base speed is 3000 rpm. As described in the case set-up, the loss model implemented is mathematical for the hysteresis and excess loss coefficients and therefore a loss separation would not be accurate from a physical perspective. Thus, the focus in this section will be on the total iron losses.

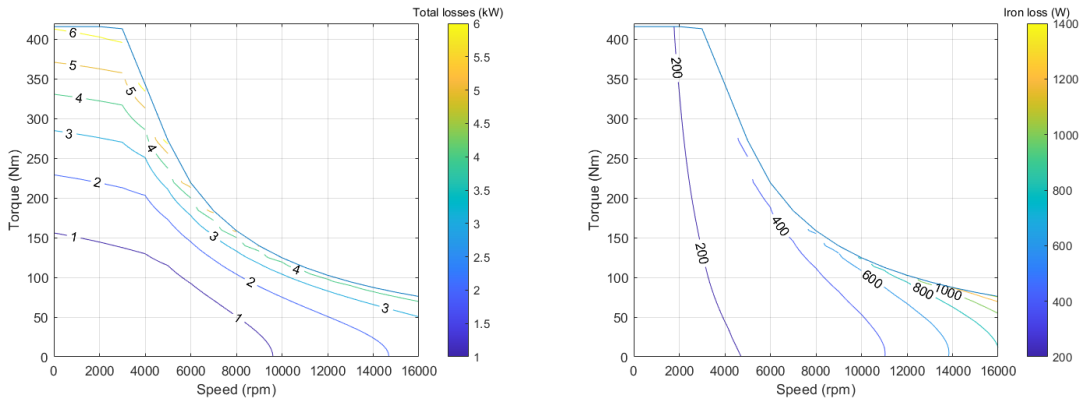

Figure 5.1: Total loss and total iron loss of the EM with non-degraded punched NO25 material and sinusoidal feeding.

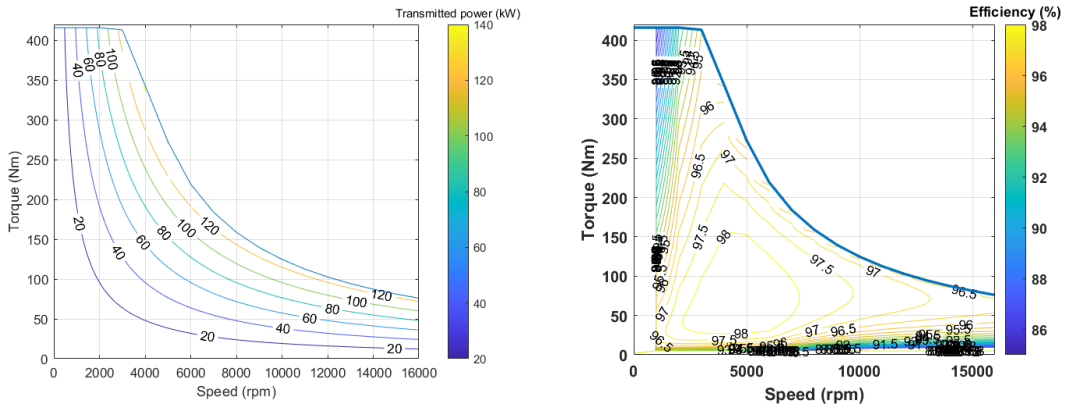

Figure 5.2: Transmitted power and efficiency of the EM with non-degraded punched NO25 material and sinusoidal feeding.

In Table 5.1, the iron loss and efficiency for each of the four materials at 3000 rpm, or 200 Hz, and 100 Nm torque can be seen. The difference between the degraded and non-degraded case for the punched and laser cut NO25 is also presented in the table. For the punched material, the degraded EM has 14 % higher iron losses and 0.09 percentage points lower efficiency than the non-degraded simulation. The substantial difference in iron loss results in a smaller change in efficiency since the copper losses are higher than the iron losses so even though the iron losses change, the total losses do not change that much. For the laser cut sample, the iron losses are increased by 15.6 % and the efficiency is decreased by 0.12 percentage points for the degraded EM. As expected from the measurements results, the degradation effects are higher for the laser cut material than for the punched one.

Table 5.1: Core loss and efficiency of the EM and the difference between degraded and non-degraded materials for punched and laser cut NO25 at 3000 rpm and 100 Nm with sinusoidal feeding.

Material	P_{core} [W]	P_{core} diff [%]	η [%]	η diff [%]
Non-degraded Punched NO25	179.6	-	97.99	-
Degraded Punched NO25	204.7	14.0	97.90	-0.09
Non-degraded Laser Cut NO25	210.6	-	97.89	-
Degraded Laser Cut NO25	243.5	15.6	97.77	-0.12

Table 5.2 shows the iron losses and efficiency of the four simulated EMs at 3000 rpm and 250 Nm. The results show a similar behavior as the previous operating point. For the punched NO25, the difference in iron loss is 12.6 % and the difference in efficiency is 0.06 percentage points. For the laser cut material, the iron loss difference is 13.9 % and the efficiency difference is 0.07 percentage points. So once again, the laser cut material has a higher degradation effect than the punched material.

Table 5.2: Core loss and efficiency of the EM and the difference between degraded and non-degraded materials for punched and laser cut NO25 at 3000 rpm and 250 Nm with sinusoidal feeding.

Material	P_{core} [W]	P_{core} diff [%]	η [%]	η diff [%]
Non-degraded Punched NO25	273.0	-	96.66	-
Degraded Punched NO25	307.5	12.6	96.60	-0.06
Non-degraded Laser Cut NO25	317.1	-	96.61	-
Degraded Laser Cut NO25	361.1	13.9	96.54	-0.07

The iron losses and efficiencies of the four simulated EMs at 9000 rpm, 600 Hz, and 100 Nm are presented in Table 5.3. Since the simulation was run at 200 Hz, this operating point has been interpolated and may not be as accurate. Further, the loss model and BH curves of the material are from measurements at 200 Hz. The iron loss difference between the non-degraded and degraded EM for the punched material is 24.1 % and the difference in efficiency is 0.11 percentage points. The EM with the laser cut material has an increase in iron loss of 15.2 % and the decrease in efficiency is 0.11 percentage points. At this speed, the results show that the loss increase is higher for the punched material than the laser cut material. That is unexpected since the measurements show that the laser cutting leads to higher degradation effects than punching.

Table 5.3: Core loss and efficiency of the EM and the difference between degraded and non-degraded materials for punched and laser cut NO25 at 9000 rpm and 100 Nm with sinusoidal feeding.

Material	P_{core} [W]	P_{core} diff [%]	η [%]	η diff [%]
Non-degraded Punched NO25	448.2	-	97.52	-
Degraded Punched NO25	556.3	24.1	97.41	-0.11
Non-degraded Laser Cut NO25	659.6	-	97.30	-
Degraded Laser Cut NO25	760.1	15.2	97.19	-0.11

6
Discussion

Something to take into consideration when analysing the results from this project is that some measurements were taken with an Epstein frame while others were taken using an SST. The Epstein frame is more accurate in general and was therefore used for as many measurements as possible but the SST was used when there were not enough samples. The degradation behavior can be seen even though the results from the Epstein frame and SST may differ some from each other. However, it is good to consider this factor, especially in cases where results are very close to each other. Further, both the Epstein frame and SST have measurement uncertainties in the equipment and do not give exactly the same results each time they are used.

The results show that the loss for PWM feeding are significantly higher than for sinusoidal feeding. The increase in loss is due to the ripple occurring in the field strength and flux density, but it is interesting that the loss is lower when it is recreated with sinusoidal data. Only the low order harmonics were included in the recreation since the higher order harmonics resulted in so low B-peaks that they were hard to include. The loss would increase a bit more if all of them were included, however it is hard to determine if it would add up to the same loss as for PWM. It is also noticeable that the higher frequency modulation ratios have a larger difference to the recreation than what the lower do. This is however reasonable since higher order harmonics could be included for lower frequency modulation ratios.

The difference in loss between PWM feeding and sinusoidal feeding were unexpectedly high. This might be due to how the PWM feeding is utilized and controlled in the measurement equipment. In the measurement, a certain B-value is chosen and then H is fed to obtain and control that B-value. From the time dependent plots in section 4.4.1 the H curve had higher ripple than B had, an especially high difference could be observed between the ripple for f_r=99 and 199. The way that the signal is controlled might give rise to higher losses than it does in the EM where a certain voltage is fed to the EM and the B-value is more of a result rather than a set value. This might explain why the expected iron loss difference in the EM is much lower than the difference that is being measured. It might also be an explanation to why the recreated power loss becomes lower, especially since the ripple in H is proportionally higher for f_r=99 and 199 which are more off in the recreation. It would be interesting to implement the PWM feeding in FEM simulations and evaluate the difference in iron loss in the EM. The difference in the EM might be lower than it is for measurements of the material.

Another interesting evaluation for the PWM feeding would be to measure on higher frequencies. It is clear that the iron losses have a big dependency of the frequency and a higher fundamental frequency could maybe impact the difference between sinusoidal feeding and PWM feeding. The eddy currents loss become higher and more dominating for higher frequencies which might have an impact on the results. It is however not that probable that it would influence the degradation more than for sinusoidal feeding since PWM do not seem to have extra influence on the degradation.

An interesting result from the degradation comparison for different materials is that some materials had better magnetic properties but were more affected by degradation and some materials had worse magnetic properties but were less affected by degradation. In areas close to the cut edge, where the degradation effects are most significant, it might be better to have a material with worse magnetic properties if it is less affected by degradation. That is because the degraded material may have better properties than a different material that has better properties in the non-degraded case but is more affected by degradation. This becomes particularly important for applications where the EM is smaller and has shorter distances to cut edge.

6.1 Modelling

When obtaining the results that show the degradation vs. the distance to the cut edge, the distance refers to the width measured from the center of the sample to the cut edge. The degradation at 5 mm for example is the measured degradation for sample C, which is not exactly the degradation observed at 5 mm from the cut edge. This is more of an averaged value of degradation since the measurement also include the effect closer to the cut edge, where the degradation is clearly much higher. Therefore, the narrower the sample, the more accurate and precise are the measurement of the degradation at a specific point. The results show that there are degradation effects at 5 mm from the cut edge, but since we know that the degradation is much higher close to the cut edge and that the measurement includes that effect as well, it is probable that the actual degradation effect at 5 mm is much lower.

To get a more accurate value for the degradation at the specific distance from the cut edge some kind of difference from the narrower sample should be taken into consideration. By excluding the degradation close to the edge we get a better understanding of how much the material are effected further into the material. Another model approach could be to divide the EM into sections which all have a width that can be represented by a sample. In that way, the averaged values would be more representative of the degradation happening over the area where it is applied. It should however be avoided to divide the core into multiple strips from the cut edge and then apply the degradation results from this thesis since that would mean that the degradation close to the cut edge are implemented for each strip which would result in a too high degradation.

For this thesis, sample A was used as the reference case and was considered non-degraded. From the comparison with the data sheet however, it could be seen that sample A differed from the data sheet, meaning that it is not actually completely non-degraded. Using a wider sample than 30 mm as the non-degraded case could be more accurate but since the maximum width of samples for the measuring equipment used was 30 mm, this was chosen to be considered the non-degraded case. Further, since the measurements are average values, the actual degradation at 15 mm from cut edge, the center of sample A, is probably not as high as the measurements are showing.

When modelling the iron losses with the Bertotti model, the hysteresis and excess loss coefficients are obtained mathematically by curve fitting. This means that the loss separation was not modelled, since there is no physical connection for these coefficients. Therefore, only the total iron losses could be studied and not the proportions between the different types of losses. It would have been interesting to see how each of the parts of the iron losses are affected by the factors considered in this thesis.

A limiting factor when it comes to the modelling in this thesis is that the models had to be implementable in Ansys Maxwell. For the loss modelling, Ansys uses the Bertotti model to compute iron losses in the EM simulations so to implement a different model may not be possible. For the degradation model, it would have been more accurate to have a model that shows the instantaneous degradation instead of the average value. However, that would not have been possible to implement in Ansys since there is no way to continuously change the material properties, the model has to be divided into segments with different material properties. These limitations had to be considered for the modeling throughout the report and if they had not existed, maybe a different approach would have been used.

For the simulations of the EM, some simplifications were made. Firstly, only the degradation on the stator was considered and the degradation in the rotor was excluded. Most of the iron losses are from the stator which is why this simplification was done but to have a more precise simulation, the degradation in the rotor should also be included. Another simplification is that the mapping of the EM was done from a simulation at 200 Hz and then values were interpolated for the other speeds. This means that the results presented for the operating point at 9000 rpm, or 600 Hz, are interpolated values and may not be as accurate as the results for the operating points at 200 Hz. It would have been beneficial to run the simulation at 600 Hz as well to see how the results would have differed since the BH curve and loss model is affected by the frequency. It is unexpected that the iron loss increase is higher for the punched material than the laser cut material for the operating point at 600 Hz. The reason for this is currently unknown but it could be due to the interpolation or loss model. It would be interesting to perform a simulation for each frequency in the torque speed map to see the full effect of the degradation on the EM with fewer interpolations.

Throughout the thesis, there have been a number of uncertainties and simplifications. The measurements have uncertainties from the equipment and also from that the measurements were taken with two different measurement devices. Then, these measurements with uncertainties were used to model the degradation and loss and the models are simplifications that differ some from the measurements. Then these models are simplified further in the FEM simulations to see what the degradation effects are on a system level. All of these uncertainties should be kept in mind since they affect the results when they are added together. It seems that the general behavior of the degradation effects are consistent but the actual values obtained are probably not completely accurate.

6.2 Ethics and sustainability

An important factor when it comes to ethics and sustainability is the accuracy of simulations of EMs. As previously mentioned, the electric vehicle industry has developed and expanded recently and there is a demand for high efficiency EMs. However, saying an EM has higher efficiency than it does causes problems. It is important with high accuracy regarding the EM efficiency for efficient use of resources to minimize the environmental impact. It is also important for the transparency from the businesses to uphold ethical standards and giving trust.

The accuracy of the iron losses also contributes to understanding how the efficiency of the EM is affected by design choices. More precise modelling of iron losses also contributes to the understanding of the loss which could help when trying to reduce the loss.

Several factors regarding ethics and sustainability can be impacted by the manufacturing process of the iron sheets in the EM. For example, punching produces more material waste than laser cutting and therefore utilizes the resources more poorly. On the other hand, laser cutting generally requires more energy than punching due to the high power needed for the laser source and can therefore have more impact on the environment.

7
Conclusion

The purpose of this thesis was to analyse and compare iron loss degradation due to different manufacturing methods and flux distributions. This was to be done by carrying out measurements and implementing the results in a FEM simulation in Ansys Maxwell. Conclusions were drawn from the comparison between different materials and cutting methods, from the comparison between sinusoidal and PWM feeding, and from the simulation of the EM.

For the comparison between different materials, three main comparisons were made. These were between punched and laser cut materials, between samples cut in the transversal and length directions, and between thinner and thicker steel sheets. It is apparent that all investigated materials are affected by degradation due to manufacturing. It can be concluded that the punched materials have better magnetic properties and also have lower degradation than laser cut materials. The relative permeability was around 50 % lower for the laser cut material than for the punched material and the specific power loss was up to 80 % higher for the laser cut material at low B-values. The materials cut in the length direction have better magnetic properties, but are more affected by degradation than the ones cut in the transversal direction. For the cross cut samples, the relative permeability was up to 60 % lower than for the length cut samples. The thinner material has better magnetic properties than the thicker material but the thicker material has a lot lower degradation. Further, if all measured materials are compared, the NO27 material cut with punching in the length direction is the material with the best properties.

Measurements on PWM feeding were done to evaluate the effect of non-sinusoidal flux distributions. The measurements were done for one fundamental frequency, five different frequency modulation ratios and three different modulation indices. It could be concluded that there was a substantial difference in power losses between PWM feeding and sinusoidal feeding. The percentage difference ranged from 120 % for low flux densities and high f_r, up to as much as 750 % for high flux densities and low f_r. When comparing different f_r it showed that higher f_r yields a lower specific power loss and regarding m_a, higher m_a gives the lowest power loss. When it comes to degradation, PWM feeding does not have an extra effect and it appears similar to the degradation for sinusoidal feeding. The degradation for PWM feeding is even a bit lower for some distances from the cut edge.

For the modelling of the degradation, the measured loss and field strength curves were curve-fitted to an exponential function and the largest error between measured and modeled values was 2.3 % for H and 6 % for P_s. The model was implemented in a FEM simulation by putting a degraded material in a segment from the cut edge to 1 mm from the cut edge. The losses were modelled using the Bertotti model with one set of coefficients for each frequency. Simulations were done with laser cut and punched materials to see the degradation effects in an EM. It can be concluded that for both punched and laser cut materials, the iron losses were increased and the efficiency was decreased in the degraded case compared to the non-degraded case. The amount of change depended on the operating point. For the punched material, the iron losses increased by 12.6-24.1 % and the efficiency decreased by up to 0.11 percentage points. The iron losses for the degraded laser cut material increased by 13.9-15.6 % and the efficiency decreased by up to 0.12 percentage points.

7.1 Future work

For future development and further understanding of the degradation effects on EMs due to manufacturing, there are several additional steps that could be done. It would be interesting to do simulations with PWM feeding to see what the degradation effects look like on a system level. Measurements with PWM could also be done at higher frequencies. The comparison of degradation could have been more accurately analysed if all samples were measured in the Epstein frame. The degradation model could be improved by having instantaneous values instead of the average degradation that is used in this thesis since that could lead to more precise modelling. For the loss modelling, a model with more physical meaning could be developed in order to make it possible to separate the different types of iron losses to see how each type of loss is affected by degradation. When it comes to the simulations, a full mapping with simulations run at each speed would be interesting to see the degradation effects on the whole operating range of the EM. The degradation in the rotor could also be considered to get more accurate results. Finally, more steps in the manufacturing process and manufacturing methods could be analysed and compared.

References

[1] S. Bakken, *Transport and mobility*, 2023. [Online]. Available: https://www.eea.europa.eu/en/topics/in-depth/transport-and-mobility?activeTab=fa515f0c-9ab0-493c-b4cd-58a32dfaae0a.

[2] S. Soltanipour, T. Thiringer, and J. Lindström, "Battery electric vehicle performance evaluation by considering punching effect on pmsm iron cores," in *2022 International Conference on Electrical Machines (ICEM)*, 2022, pp. 2162–2168. DOI: 10.1109/ICEM51905.2022.9910633.

[3] M. Oka, H. Kiyotake, M. Enokizono, and D. Wakabayashi, "Iron loss measurements under pwm excitation for ring cores made of ultrathin electrical steel sheets for a stator core," in *2020 International Conference on Electrical Machines (ICEM)*, vol. 1, 2020, pp. 2294–2300. DOI: 10.1109/ICEM49940.2020.9270980.

[4] *IEC 60404-2*. The International Electrotechnical Commission, 2008.

[5] A. A. Mohammadi, S. Zhang, A.-C. Pop, and J. J. C. Gyselinck, "Effect of electrical steel punching on the performance of fractional-kw electrical machines," *IEEE Transactions on Energy Conversion*, vol. 37, no. 3, pp. 1854–1863, 2022. DOI: 10.1109/TEC.2022.3158394.

[6] A. Krings, "Iron losses in electrical machines — influence of material properties, manufacturing processes, and inverter operation," Ph.D. dissertation, KTH School of Electrical Engineering, 2014.

[7] A. Boglietti, A. Cavagnino, T. Mthombeni, and P. Pillay, "Comparison of lamination iron losses supplied by pwm voltages: Us and european experiences.," in *2005 IEEE International Conference on Electric Machines and Drives*, 2005, pp. 1431–1436.

[8] V. Lidskog, *Experimental magnetic and iron loss degradation in elecrical machines*, 2023.

[9] V. Leivsdottir, *Investigation of loss calculation methods for pmsms and implementation of loss functionality on a developed fem model*, 2016.

[10] E. Campara and A. Solakovic, *Iron loss modelling for a permanent magnet synchronous motor*, 2020.

[11] D. Ribbenfjärd, "Electromagnetic transformer modelling including the ferromagnetic core," Ph.D. dissertation, Kungliga Tekniska Högskolan, 2010.

[12] B. Koprivica, A. Milovanovic, and M. Plazinic, "Standard methods of measurement of the magnetic properties of electrical steel strip and sheet," in *XI International Systems, Automatic Control and Measurements Conference*, 2012, pp. 298–301.

[13] *IEC 60404-3*. The International Electrotechnical Commission, 2010.

[14] H. Wang and Y. Zhang, "Modeling of eddy-current losses of welded laminated electrical steels," *IEEE Transactions on Industrial Electronics*, vol. 64, no. 4, pp. 2992–3000, 2017. DOI: 10.1109/TIE.2016.2636203.

[15] M. Bali, H. De Gersem, and A. Muetze, "Finite-element modeling of magnetic material degradation due to punching," *IEEE Transactions on Magnetics*, vol. 50, no. 2, pp. 745–748, 2014. DOI: 10.1109/TMAG.2013.2283967.

[16] V. M. Paltanea, G. Paltanea, and H. Gavrila, "Some important effects of the water jet and laser cutting methods on the magnetic properties of the non-oriented silicon iron sheets," in *2015 9th International Symposium on Advanced Topics in Electrical Engineering (ATEE)*, 2015, pp. 452–455. DOI: 10.1109/ATEE.2015.7133856.

[17] S. Dadvandipour, "On the experimental study of electric discharge machining (edm) of p20 type tool steel," in *2013 IEEE 11th International Symposium on Applied Machine Intelligence and Informatics (SAMI)*, 2013, pp. 245–248. DOI: 10.1109/SAMI.2013.6480984.

[18] R. Sundaria, A. Lehikoinen, A. Arkkio, and A. Belahcen, "Effects of manufacturing processes on core losses of electrical machines," *IEEE Transactions on Energy Conversion*, vol. 36, no. 1, pp. 197–206, 2021. DOI: 10.1109/TEC.2020.2999528.

[19] S. V. A. Laakso, U. Aydin, and P. Krajnik, "Verification of electric steel punching simulation results using microhardness," *The International Journal of Advanced Manufacturing Technology*, vol. 112, no. 1, pp. 2027–2036, 2021. DOI: 10.1007/s00170-020-06500-6.

[20] M. Bali and A. Muetze, "The degradation depth of electrical steel sheets due to mechanical and laser cutting," in *2017 IEEE 11th International Symposium on Diagnostics for Electrical Machines, Power Electronics and Drives (SDEMPED)*, 2017, pp. 544–549. DOI: 10.1109/DEMPED.2017.8062408.

[21] N. Boubaker, D. Matt, P. Enrici, F. Nierlich, and G. Durand, "Measurements of iron loss in pmsm stator cores based on cofe and sife lamination sheets and stemmed from different manufacturing processes," *IEEE Transactions on Magnetics*, vol. 55, no. 1, pp. 1–9, 2019. DOI: 10.1109/TMAG.2018.2877995.

[22] K. Sang-Hoon, *Electric Motor Control*. 2017.

[23] *Technical data*, 2022. [Online]. Available: https://www.media.volvocars.com/global/en-gb/models/xc60/2022/specifications.

[24] *MPG-Expert 3 - Manual*. Brockhaus Measurements, 2018.

DEPARTMENT OF ELECTRICAL ENGINEERING
CHALMERS UNIVERSITY OF TECHNOLOGY
Gothenburg, Sweden
www.chalmers.se

CHALMERS
UNIVERSITY OF TECHNOLOGY